

Level set method for atomization and evaporation simulations

Kun Luo*, Changxiao Shao, Min Chai, Jianren Fan*

State Key Laboratory of Clean Energy Utilization, Zhejiang University, Hangzhou 310027, PR China



ARTICLE INFO

Article history:

Received 11 October 2018

Accepted 6 March 2019

Available online 19 March 2019

Keywords:

Level set method

Interface capturing method

Detailed numerical simulation

Mass conservation

Spray atomization

Evaporation

ABSTRACT

Atomization and evaporation processes have extensively existed in a variety of scientific and engineering applications, such as, rain formation, spray cooling, and spray combustion in propulsion devices. In spray combustion, atomization and evaporation processes govern the resultant liquid droplet characteristics, which strongly affect the combustion efficiency and pollutant emissions. However, atomization and evaporation are very complicated processes that involve convoluted interfaces as well as the breakup and coalescence of liquid masses, together with mass and heat transfers on the interface. Deep insights into atomization and evaporation put a significant challenge to the measuring techniques due to the harsh conditions and multi-scale nature of the problem within the apparatus. With the developments of computational algorithm and computer capacity, detailed numerical simulation of the atomization and evaporation processes has been a promising tool to explore the underlying physics. Level set method is such an interface capturing method, and tremendous progresses have been made for detailed numerical simulation of atomization and evaporation over the past few decades. In this article, we attempt to review the recent progresses in the development of the level set method and its applications to atomization and evaporation. Firstly, the fundamentals of the level set method are introduced and recent advances in improving the mass conservation are emphasized. Secondly, numerical issues for detailed numerical simulation of atomization and evaporation are summarized and the strategies for treating them are highlighted. We then review the state-of-the-art progresses in detailed numerical simulation of atomization and evaporation with the level set method. The challenges and future prospects are summarized in the end.

© 2019 The Authors. Published by Elsevier Ltd.

This is an open access article under the CC BY license. (<http://creativecommons.org/licenses/by/4.0/>)

Contents

1. Introduction	66
2. Level set method	68
2.1. Basic level set formulation	68
2.2. Issues of and strategies to improve the basic level set method	69
2.2.1. Discretization of the level set equation	69
2.2.2. Extension velocity to transport level set equation	70
2.2.3. Hyperbolic tangent level set method	70
2.2.4. Interface refined level set method	71
2.2.5. Improvement of the re-initialization process	71
2.2.6. Hybrid method	72
2.2.7. Variational level set method	73
3. Level set method for atomization with evaporation	74
3.1. Governing equations	74
3.2. Numerical issues and treatments of atomization with evaporation	74
3.2.1. Interface jump conditions and their treatments	75
3.2.2. Navier–Stokes equations and divergence-free velocity extension	76

* Corresponding authors.

E-mail addresses: zjulk@zju.edu.cn (K. Luo), fanjr@zju.edu.cn (J. Fan).

3.2.3. Calculation of evaporation rate	76
4. Application of the level set method to atomization and evaporation	77
4.1. Primary atomization	77
4.2. Secondary atomization	80
4.2.1. Single droplet deformation and breakup	80
4.2.2. Droplet collision	82
4.2.3. Droplet impact on surface	83
4.2.4. Atomization with turbulence	84
4.3. Integrated simulation of atomization	84
4.4. Interface with evaporation	86
5. Summary and outlook	88
Acknowledgments	88
Supplementary material	88
Appendix A	88
Appendix B	89
Appendix C	89
References	90

1. Introduction

Gas-liquid two-phase flows with evaporation have extensively existed in a variety of scientific and engineering applications, such as spray cooling [1,2], spray combustion [3,4] and so on. Among these applications, spray combustion has attracted a lot of attention due to its paramount importance in power generation. Spray combustion can be divided into several sub-processes, such as, fuel injection, atomization, droplet dispersion, evaporation, fuel-air mixing, and combustion, as illustrated in Fig. 1. Liquid fuel is firstly injected from the nozzle in the form of bulk liquid to the combustion chamber and then is atomized into large numbers of fine droplets. The atomization process can further be divided into primary atomization and secondary atomization. The primary atomization is defined as the process from bulk liquid to filaments and droplets, and the secondary atomization is defined as the process from the filaments and droplets to much smaller droplets. After evaporation of droplets, ignition and combustion occur to provide power for the system.

To achieve optimized performance of combustion as well as low pollution emission, atomization and evaporation should be well-understood. However, atomization and evaporation are very complex processes that involve multi-scale convoluted interfaces as well as breakup and coalescence of liquid masses [5], together with heat and mass transfers on the phase interfaces. Deep insights into atomization and evaporation put a significant challenge to diagnostic technologies due to the harsh conditions and multi-scale nature of the problem within the apparatus. Taking the atomization process as an example, it is usually a problem in hydrodynamic instability and transitional turbulence, with typical multi-scale characteristics. The length scale could range from the size of the flow to the size of the smallest droplets. With the developments of computational algorithm and computer capacity, computational fluid dynamics (CFD) has been demonstrated to be an efficient tool to explore the underlying physics of atomization and evaporation. The goal of the present review is to summarize the recent progress in CFD of atomization and evaporation with the level set method.

Essentially, there are three kinds of approaches in the classical CFD of atomization and evaporation in spray combustion, *i.e.* Reynolds averaged Navier-Stokes (RANS), large eddy simulation (LES), and direct numerical simulation (DNS). It has been well-known that RANS is able to get only the time-averaged information with closure models, but the computational cost is the lowest. These features are attractive to industrial engineers. LES of atomization with sub-grid models has appeared in the recent years [6–10]. The principal idea of LES is to reduce computational cost by spatial filtering of the governing equations and introducing the

turbulent viscosity. However, there is an inherent weakness of LES of atomization, for instance, the contrary of underlying critical assumption of turbulent viscosity and the physical process of atomization. In most practices of LES, the value of the turbulent viscosity is positive by a diffusive mechanism, meaning energy transfer from resolved scales to the subgrid scales [11]. But in reality, the energy transfer is bi-directional [12]. In particular, Elghobashi and Truesdell [13,14] found the energy backscatter in particle-laden flows. Regarding DNS, all scales in the system should be resolved without closure models, particularly the Kolmogorov scale η in the gas and liquid phases, and the smallest scale of droplet need to be resolved. For the Kolmogorov scale, the spatial resolution criterion $k_{\max}\eta \geq 1.5$ [15] should be satisfied, in which k_{\max} is the maximum wavenumber. For the smallest scale of droplet, at least four to eight grid points are required to obtain a physically reasonable droplet. All these requirements lead to so huge computational demand for DNS of atomization and evaporation that usually only the gas-phase is fully solved while the liquid phase is modeled using atomization and evaporation models in the literature. In previous CFD simulations of spray combustion, atomized droplets or atomization models were commonly used [3,4,16]. However, it has been demonstrated that spray combustion characteristics can be significantly influenced by the atomization conditions [17,18]. Furthermore, though a variety of evaporation models exist, most of them are based on empirical correlations for spherical droplets [19]. To eliminate possible errors from traditional atomization and evaporation models so as to improve CFD of spray combustion, there is an urgent need to develop advanced numerical methods for better understanding and characterizing atomization and evaporation.

To this end, two-phase DNS with fully-resolved interface methods has drawn a lot of attention in the recent years. In principle, this kind of DNS can resolve all scales involved in the system. However, the smallest droplet size (the Hinze length scale) has not always been well resolved in the literature, and this method is thus usually called as detailed numerical simulation or under-resolved DNS [12]. Crucial to detailed numerical simulation of atomization and evaporation is the way to capture or track the gas-liquid interface. Basically, interface capturing denotes the Eulerian description of the interface, whereas interface tracking denotes the Lagrangian description of the interface. During the last three decades, three major interface capturing/tracking methods, namely, the front tracking method [20,21], the volume-of-fluid (VOF) method [22,23], and the level set method [24–26] have been developed. As illustrated in Fig. 2, the front tracking method is based on tracking massless particles to represent the gas-liquid interface. While the VOF method utilizes the liquid volume fraction to represent the interface. The volume fraction ϕ_{vol} is speci-

Nomenclature

Latin letters

A or a	Coefficient
C_p	Specific heat
D	Nozzle diameter
D_m	Mass diffusion coefficient
f	Forcing term
F	Propagation speed
\vec{g}	Gravitational acceleration
h_{lg}	Latent heat of evaporation
H	Heaviside function
I	Energy density function
k_{max}	Maximum wavenumber
m	Molar mass
\vec{n}	Normal vector
Oh	Ohnesorge number
p	Pressure
r	Radius
Re	Reynolds number
sgn	Signum function
t	Time
T	Temperature
\mathbf{U} or \vec{u}	Velocity
V	Volume
We	Weber number
X or \vec{x}	Location
Y	Mass fraction

Greek letters

α	Varying factor
γ	Kinetic mobility
γ_D	Droplet aspect ratio
ε	Profile thickness
η	Kolmogorov length scale
κ	Interface curvature
λ	Thermal conductivity
μ	Dynamic viscosity
ρ	Density
σ	Surface tension
τ	Fictitious time
Γ	Gas-liquid interface
$\vec{\tau}$	Deviatoric stress tensor
ϕ or G	Level set function
ϕ_{vol}	Volume fraction scalar

$\vec{\Phi}$	Level set gradient
ψ	Hyperbolic tangent function
$\dot{\omega}$	Evaporation rate
Ω	Domain

Θ	Energy functional
<i>Superscripts</i>	
t	Transpose
ghost	Ghost value

Subscripts

0	At initial time or at the reference
cf	Crossflow
ext	Extension
g	Gas
l	Liquid
p	Particle
sat	Saturation
vap	Vapor
x, y, z	x, y, z directions

Acronyms

AMR	Adaptive mesh refinement
CFD	Computational fluid dynamics
CLSOF	Coupled level set/volume-of-fluid
DG	Discontinuous Galerkin
DNS	Direct numerical simulation
ELSA	Eulerian-Lagrangian Spray Atomization
ENO	Essentially non-oscillatory
FMM	Fast marching method
GALS	Gradient-augmented level set
GFM	Ghost fluid method
HFM	Heat flux based model
HIT	Homogeneous isotropic turbulence
KH	Kelvin-Helmholtz
LES	Large eddy simulation
LPP	Lagrangian point-particle
PDE	Partial differential equation
RANS	Reynolds average Navier-Stokes
RLSG	Refined level set grid
RT	Rayleigh-Taylor
SMFM	Species mass flux based model
TAB	Taylor analogy breakup
TS	Tollmien-Schlichting
TVD	Total variation diminishing
VOF	Volume-of-fluid
WENO	Weighted essentially non-oscillatory

fied as $\phi_{vol} = 1$ for liquid, $0 < \phi_{vol} < 1$ for interface and $\phi_{vol} = 0$ for gas. In the level set method, the interface is implicitly represented as the zero iso-surface of a signed distance function ϕ , with $\phi > 0$ denotes liquid and $\phi < 0$ denotes gas. The other interface resolved methods include the Lattice Boltzmann method [27–29], the smoothed particle hydrodynamics method [30,31] and the phase field method [32,33]. The advantage and disadvantage of these interface-resolved numerical methods are summarised in Table S1. An excellent review of different interface-capturing methods can also be found in [34].

Among the interface-capturing methods, the VOF method and the level set method are the most popular methods. Some qualitative and quantitative comparisions between them have been reported. Mirjalili et al. [34] gave a comprehensive but qualitative comparison between the VOF method and the level set method. It

was shown that the level set method has the advantages of economical cost and simplicity of computing normal and curvature, while the VOF method has the advantage of mass conservation. Quantitatively, Albadawi et al. [35,36] compared the VOF method and the level set method by simulating the bubble growth and detachment at low Capillary and Bond numbers. The level set method had been shown to predict the bubble detachment volume with errors lower than 2%, better than the VOF method. Denner et al. [37] found that the level set method performs better for quasi-stationary flows where surface tension dominates, but it suffers from numerical diffusion in simulation of rising bubble. Bilger et al. [38] performed a direct and quantitative comparison of the VOF method and the level set method in the same code, and found that the VOF method shows smaller errors of spurious currents and the level set method shows a greater sensitivity to operating parame-

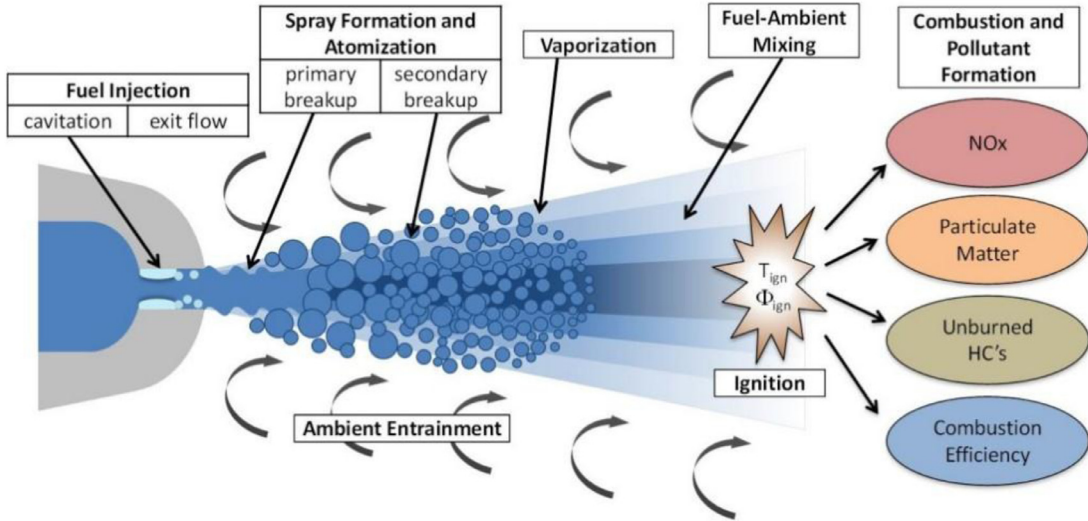


Fig. 1. A schematic of spray combustion process. Reprinted from <https://www.archie-west.ac.uk/projects/computational-fluid-dynamics/the-cfd-development-of-non-premixed-dual-fuel-combustion-diesel-engine-injected-by-high-pressure-gas-in-the-cylinder-chamber/>.

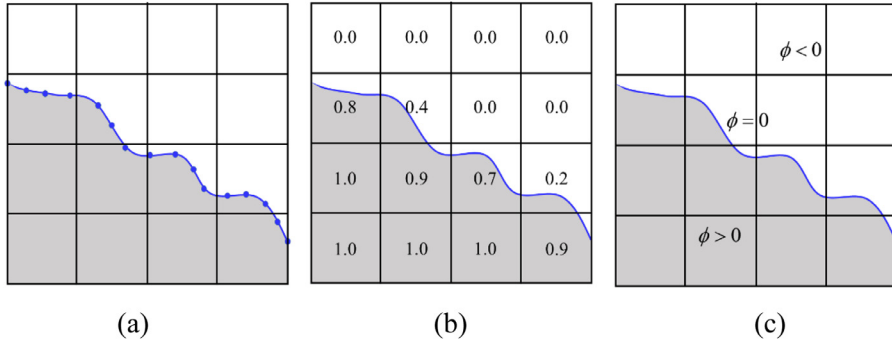


Fig. 2. Illustration of three interface tracking/capturing methods, (a) front tracking method; (b) volume-of-fluid method; (c) level set method; (Blue line represents interface, gray region represents the liquid phase, blue dots in (a) represent tracking points, the numbers in (b) represent the liquid volume fraction in each cell, and the function in (c) represents the level set function).

ters for the low Capillary number. For the high Capillary number, the level set method exhibits a slightly better ability to capture droplet pinch-off. These studies demonstrate that the VOF method and the level set method each has its unique advantage in certain regime. Due to its simplicity, the level set method has been paid numerous attention and significant progresses on atomization and evaporation have been achieved in the recent years [39,42].

The main objective of this review is to highlight the fundamental developments of the level set method, identify some numerical challenges and recent progresses, and provide future outlooks from the perspectives of detailed numerical simulation of atomization and evaporation. The feature of this review is that atomization and evaporation are formulated together in the framework of the level set method, and relevant issues and advances are comprehensively summarized. Although some relevant reviews [39–42] have been published, most of them focus on either the level set method itself or atomization models, which distinguishes them from the present review. In Section 2, we will introduce the basic level set formulation and the strategies to improve mass conservation, which is of significant importance for simulations of atomization and evaporation. In Section 3, numerical issues and strategies for simulating atomization with evaporation will be discussed. This is followed by the recent state-of-the-art progresses achieved by the level set method, including the primary atomization, the secondary atomization, the atomization with turbulence, and the evaporation in

Section 4. Finally, the challenges and future prospects in simulating atomization and evaporation processes with the level set method will be outlined.

2. Level set method

2.1. Basic level set formulation

Description of the interface evolution is a fundamental component of gas-liquid flows. The level set method proposed by Osher and Sethian [26] is an efficient way to represent the interface as the level set of a higher dimensional function. It has evolved from a mathematical formulation to a versatile and powerful methodology for interface capturing [39–42]. The main advantage of this implicit representation of a moving interface is its ability to naturally handle topology changes, as shown in Fig. 3. The basic level set formulation is introduced as follows.

The level set method represents the interface, Γ , as the zero-contour of a higher dimensional function, ϕ , called the level set function, which is usually defined as the signed distance function to Γ :

$$|\phi(\vec{x}, t)| = |\vec{x} - \vec{x}_\Gamma|, \quad (1)$$

where \vec{x}_Γ is the location on the interface that is closest to \vec{x} , and ϕ takes positive values on one side of the interface and negative

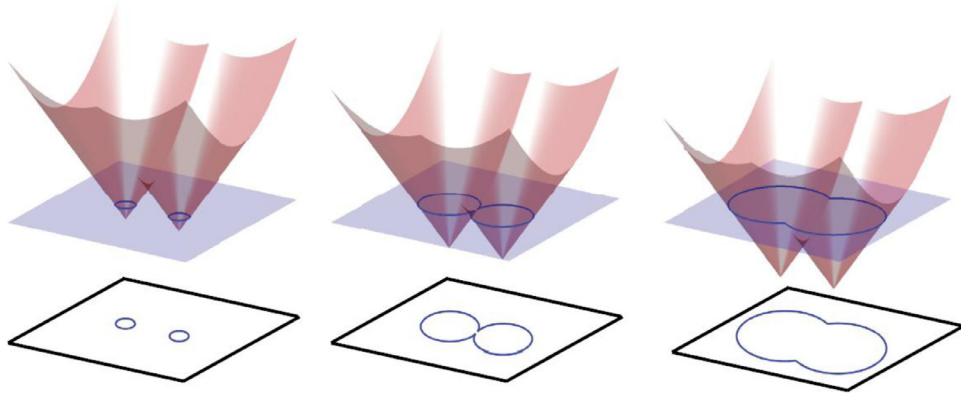


Fig. 3. Level set representation of a two-dimensional free boundary (blue solid line) moving in its normal direction, and subsequent changes in topology that are handled automatically. The level set function is depicted in red color. Reprinted from Gibou et al. [40] with permission of Elsevier. (For interpretation of the references to color in this figure legend, the reader is referred to the web version of this article.)

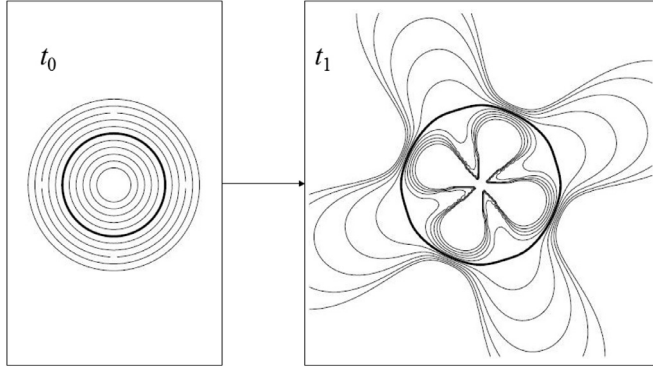


Fig. 4. Level set function without re-initialization from time t_0 to t_1 under certain velocity field (the thick lines represent the interface and the thin lines represent iso-surface of the level set function). Reprinted from Sethian [44] with permission of Cambridge University Press.

values on the other side. The interface normal vector \vec{n} and the interface curvature κ are easy to be calculated as:

$$\vec{n} = \frac{\nabla\phi}{|\nabla\phi|} \text{ and } \kappa = -\nabla \cdot \vec{n}. \quad (2)$$

Under a velocity field $\vec{u} = (u, v, w)$, the interface evolves according to the level set transport equation:

$$\frac{\partial\phi}{\partial t} + \vec{u} \cdot \nabla\phi = 0. \quad (3)$$

Since the level set function does not retain its signed distance function property as it evolves in time as illustrated in Fig. 4, Sussman et al. [43] introduced the re-initialization equation

$$\phi_\tau + \text{sgn}(\phi_0)(|\nabla\phi| - 1) = 0 \quad (4)$$

to transform a level set function ϕ_0 into the signed distance function ϕ . Here, sgn is a smoothed-out signum function and τ represents a fictitious time that controls the width of the band around the zero-level set where ϕ will be sign-distaned.

2.2. Issues of and strategies to improve the basic level set method

Despite of inherent advantages, the level set method suffers from unphysical loss of the fluid mass as time evolves, which is a crucial issue to detailed numerical simulation of atomization and evaporation. There are two main reasons for the mass loss in the

existing level set method. Firstly, the discretization of the level set equation may lead to significant numerical dissipation that usually manifests itself as a loss of mass in the areas of high curvature or other under-resolved regions [39]. Secondly, in the re-initialization process, the zero level set can be altered owing to numerical artifacts, which leads to additional mass loss. Numerous attempts have been made to improve the mass conservation property of the basic level set method, which can be classified into seven categories as follows.

2.2.1. Discretization of the level set equation

As one part of the numerical error comes from the discretization of the level set equation, it is straightforward to improve the accuracy by increasing the order of discretization schemes. Since the level set transport equation is a hyperbolic equation ($\phi_t + \vec{u} \cdot \nabla\phi = 0$), a rich class of classical algorithms are available for its discretization, including the upwind scheme, the MacCormack method, the Essentially Non-Oscillatory (ENO) scheme, the Weighted Essentially Non-Oscillatory (WENO) scheme, the total variation diminishing (TVD) method, etc. Nourgaliev et al. [45] used 5th-order linear WENO scheme to discretize the level set equation and pointed out that mass losses are reduced compared to lower order scheme. Salih et al. [46] examined the first-order upwind scheme, the MacCormack method, the second-order ENO scheme and the fifth-order WENO scheme, and demonstrated that the level set method performs better when high-order schemes are used.

Recently, other preserving schemes have been developed for the level set formulation. Sheu et al. [47,48] proposed a dispersion relation preserving advection scheme [47]. This scheme maintains a sharp shape of the level set profile to promote good mass conservation, and excellent agreement with experimental data can be achieved. Another popular numerical scheme is the Discontinuous Galerkin (DG) method. The DG method was originally proposed by Reed and Hill [49] and has been used wildly in the discretization of the level set equation because it is a compact scheme with arbitrary high-order accuracy without the necessity of a large stencil [50–53]. The main idea of the DG method is to represent a function using a linear combination of P basis functions within each cell to create a piecewise polynomial representation of the function. The semi-Lagrangian approach has also been developed for the discretization of the level set function by using an efficient, first-order accurate semi-Lagrangian advection scheme in [54,55] or a high-order scheme in [56]. However, the semi-Lagrangian advection scheme does not have the inherent conservation property, and

a discrete set of particles arriving at the grid points [57] or the particle on the interface [54] are usually used to conserve the mass conservation property.

Another high-order scheme is the so-called gradient-augmented level set (GALS) method. It is optimally local and the sub-grid structure is represented to high-accuracy since the level set function and its gradient are addressed within each cell. Defining the gradient as $\vec{\phi} = \nabla\phi$, the following equation is also solved in the GALS method,

$$\vec{\phi}_t + \vec{u} \cdot \nabla \vec{\phi} = -\nabla \vec{u} \cdot \vec{\phi}, \quad (5)$$

where $\nabla \vec{u}$ is the velocity deformation matrix. Numerical studies showed that the GALS method conserves mass much better than the standard level set method [58,59]. Based on the gradient form of the advection equation, Kohno and Nave [60] further presented a novel numerical method for resolving the level set function by using the hierarchical-gradient truncation and remapping technique.

Although numerous efforts have been made to improve the discretization of the level set equation, the mass conservation is still an issue for simulations of certain type of shearing and vortical velocity fields even by using the above-mentioned high-order and preserving schemes.

2.2.2. Extension velocity to transport level set equation

Instead of using high-order discretization of the level set equation, Adalsteinsson and Sethian [61] proposed that the level set equation can be transported by an extension velocity rather than the fluid velocity. This idea was founded on the fact that the gradient of the level set function grows very rapidly with time in shearing velocity fields. To maintain a signed distance function, the velocity field can be specially constructed so that $|\nabla\phi|=1$ and $\nabla F_{ext} \cdot \nabla\phi=0$ are satisfied, where F_{ext} is the extension velocity. It can be more precise by rewriting the level set transport equation as

$$\phi_t + F_{ext} |\nabla\phi| = 0 \quad (6)$$

Here the extension velocity F_{ext} is a certain velocity field which, at the zero level set, equals the propagation speed of the interface F , as shown in Fig. 5. The Fast Marching Method (FMM) [61] is an efficient method to construct the extension velocity field, which advances the solution from the interface in an upwind fashion.

It should be noted that this extension velocity method theoretically preserves the signed distance function without the need of re-initialization. However, the original extension velocity is only first-order approximation of the velocity field near the interface, and it may lead to unexpected numerical artifacts due to the strict

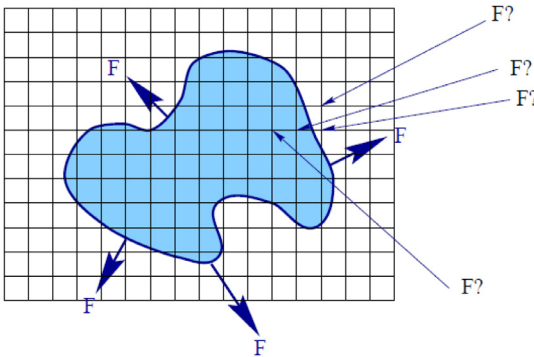


Fig. 5. Constructing extension velocities, where F is interface velocity, $F?$ is the unknown extension velocity. Reprinted from Adalsteinsson and Sethian [61] with permission of Elsevier.

requirement of the local solutions for the flow near the interface [53].

Similar to the extension velocity, Ovsyannikov et al. [62] proposed to maintain the signed distance function by introducing a source term directly into the level set equation, which has been recently extended to higher-order accuracy [63]. In this method, the level set transport equation is rewritten as

$$\frac{\partial\phi}{\partial t} + \vec{u} \cdot \nabla\phi = A(\vec{x}, t)\phi, \quad (7)$$

where the coefficient $A(\vec{x}, t)$ is an arbitrary regular function which does not depend on $\phi(\vec{x}, t)$. Through theoretical analysis, the source term could be expressed as

$$A(\vec{x}, t)\phi = [u_k - (u_k)|_{n=0}] \frac{\partial\phi}{\partial x_k}. \quad (8)$$

The Taylor's expansion of $A(\vec{x}, t)$ can be derived as an arbitrary high-order approximate form, for example, up to the second-order term as

$$A(\vec{x}, t) = A_0 + A_1 n + A_2 n^2 + O(n^3). \quad (9)$$

Application of this method simplifies the realization of the level set method in comparison with the extension velocity method, but it requires the return to the re-initialization process. Nevertheless, the number of re-initializations can be substantially reduced. Unfortunately, this method has not yet been evaluated in more complex configurations.

2.2.3. Hyperbolic tangent level set method

The level set function is not necessarily the signed distance function. When choosing a suitable level set function, three criteria should be satisfied: conservative, no spurious oscillations and constant thickness of the interface. Instead of the signed distance function, Olsson et al. [64,65] proposed to use the hyperbolic tangent function as the level set function. It is of second-order accuracy and satisfactory of mass conservation in the region bounded by the interface. The hyperbolic tangent function is defined as

$$\psi(\vec{x}, t) = \frac{1}{2} \left(\tanh \left(\frac{\phi(\vec{x}, t)}{2\varepsilon} \right) + 1 \right), \quad (10)$$

where ε is a parameter to control the thickness of the profile. This formulation constructs the correlation between the level set function and the hyperbolic tangent function. Rather than defining the interface by the iso-surface $\phi=0$, it is now defined by the location

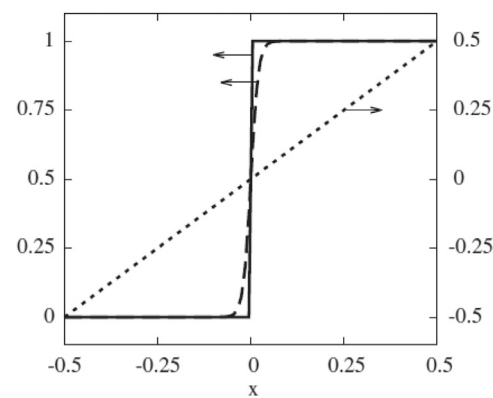


Fig. 6. Liquid volume fraction, hyperbolic tangent function, and signed distance level set function represented by solid, dashed, and dotted lines, respectively with the liquid-gas interface located at $x=0$. Reprinted from Owkes and Desjardins [52] with permission of Elsevier.

of the iso-surface $\psi = 0.5$, as shown in Fig. 6. The corresponding re-initialization equation is written as

$$\frac{\partial \psi}{\partial \tau} + \nabla \cdot (\psi(1-\psi)\vec{n}) = \nabla \cdot (\varepsilon(\nabla \psi \cdot \vec{n})\vec{n}). \quad (11)$$

This re-initialization equation is advanced in pseudo-time τ . It consists of a compression term on the left hand side that aims at sharpening the interface profile, and a diffusion term on the right hand side that ensures the profile to remain characteristic thickness ε . Through this hyperbolic tangent level set method, the mass loss can be considerably reduced [66–69].

However, this method also reduces the sharpness of the level set method in spite of its roughly conservative property. It can lead to small pieces of fluid called flotsam and jetsam non-physically breaking off from the interface in under-resolved regions and moving around with erroneous velocity, like the VOF method to some extent [68].

2.2.4. Interface refined level set method

As the level set function only needs to be resolved near the interface, the computational cost can be largely reduced by using the narrow band method [68]. But it still suffers from mass loss in the under-resolved regions. Several spatially adaptive methods have been developed to efficiently resolve the interface, including the adaptive level set approach [70,71], the octree based methods [39], the structured adaptive mesh refinement [45], the spectrally refined interface approach [57] and the refined level set grid (RLSG) method [72]. Although these variants of level set method are different in form and implementation, they all have the same essence to increase the sub-cell resolution near the interface. Consequently, the RLSG method is selected as a typical technique to be introduced here. Other spatially adaptive variants could be found in the previous reviews of Losasso et al. [39] and Gibou et al. [40], and the references therein.

The RLSG method is proposed by Herrmann [72]. The key idea of the RLSG method is to solve all level set method related equations on an additional, separate, equidistant, Cartesian grid, termed G-grid. Since both grids, the G-grid and the flow solver grid are separate, the G-grid can be independently refined to ensure a grid converged interface representation. On the first level, the flow solver grid is overlaid by an equidistant Cartesian super-grid including computational domain where the interface might exist, as shown in Fig. 7. Only those cells containing part of the interface or are within a predefined distance from the interface are activated. On the second level, each active block contains an equidistant Cartesian grid of grid cell size h_G . Again, only those cells containing part of the interface or are within a predefined distance

from the interface are activated. This approach effectively reduces the number of cells and allows for high resolution of the interface, as only small fraction of cells that are located in a small band around the interface are active and stored. For example, considering a super-grid of size 128^3 and a local block size of 32^3 , this approach yields a theoretical maximum resolution of about 70 billion cells.

Such interface refined level set methods are expected to be not only an excellent way to reduce the mass loss, but also a promising tool for multi-scale simulations of atomization and evaporation. However, challenges arise during the procedure of coupling the level set method with the hierarchical data structure. Furthermore, the parallel load balancing is of importance owing to the non-uniform grid population.

2.2.5. Improvement of the re-initialization process

The re-initialization is required in order to maintain the level set function as a signed distance function. Specifically, the re-initialization process should modify the level set function so that $|\nabla \phi| = 1$ is satisfied and keep the zero iso-surface ϕ_0 invariant. There are two major numerical approaches for the re-initialization process, namely, the partial differential equation (PDE) based approach and the FMM based approach. For each approach, improvements have been made in the literature.

The PDE based re-initialization procedure was originally proposed by Sussman et al. [43] by solving the equation $\phi_\tau = L(\phi_0, \phi) = \text{sgn}(\phi_0)(1 - |\nabla \phi|)$ to steady state. The signum function sgn is used to keep ϕ_0 unchanged on the interface. For numerical purpose, it is useful to smooth the sign function as

$$S_\varepsilon(\phi_0) = \frac{\phi_0}{\sqrt{\phi_0^2 + \varepsilon^2}}. \quad (12)$$

At steady state, ϕ will converge to $|\nabla \phi| = 1$. A nice feature of this formulation is that the re-initialization procedure completely avoids detecting the interface, which is efficient for implementation.

In complex simulations of, for example, atomization and evaporation where the interface deforms frequently and severely, this re-initialization process, however, may cause unphysically mass loss at each time step due to numerical diffusion. To conserve the volume of the domain bounded by the interface, Sussman and Co-authors [73,74] further proposed a constraint by requiring

$$\partial_t \int_{\Omega} H(\phi) = 0, \quad (13)$$

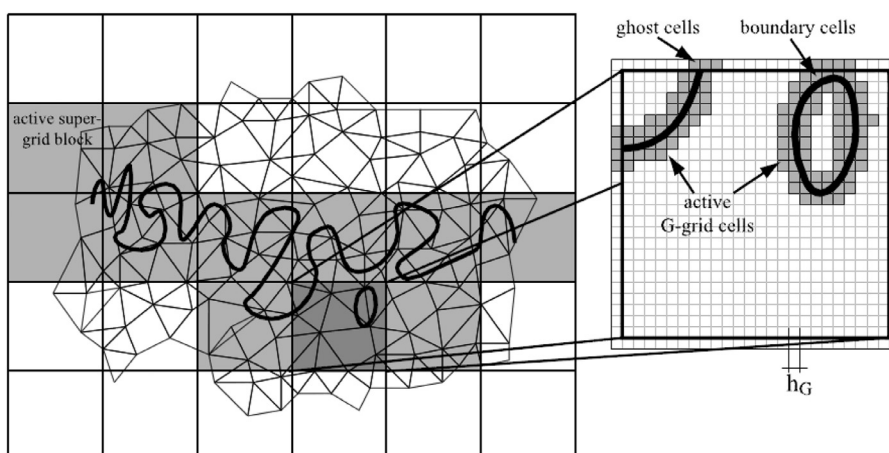


Fig. 7. RLSG grid definitions, where h_G is the grid size. Reprinted from Herrmann [72] with permission of Elsevier.

where H is a smoothed out approximation of the sign function and can be written as

$$H_\varepsilon(\phi) = \begin{cases} \frac{1}{2} & \text{if } \phi > \varepsilon \\ -\frac{1}{2} & \text{if } \phi < -\varepsilon \\ \frac{1}{2}\left(\frac{\phi}{\varepsilon} + \frac{1}{\pi} \sin(\pi\phi/\varepsilon)\right) & \text{otherwise} \end{cases} \quad (14)$$

The re-initialization equation can then be modified as

$$\phi_\tau = L(\phi_0, \phi) + Af(\phi), \quad (15)$$

where A is a function of time only and can be calculated as

$$A = \frac{-\int_{\Omega} H'(\phi)L(\phi_0, \phi)}{\int_{\Omega} H'(\phi)f(\phi)}. \quad (16)$$

The discretization scheme for the above re-initializations is found to be important to the mass conservation [75]. Hartmann et al. [76] proposed two formulations of the re-initialization scheme. One uses the least-squares method to explicitly minimize the displacement of the zero level set and the other is derived by systematically minimizing the number of constraints imposed on the re-initialization scheme. Furthermore, Hartmann et al. [77] proposed a new constrained re-initialization equation incorporating a forcing term which can be written as

$$\phi_\tau + \text{sign}(\phi_0)(|\nabla\phi| - 1) = \alpha f \quad (17)$$

where α is a weighting factor set $\alpha = 0.5$ and f is the forcing term. Indeed, this formulation combines the simplicity and generality of the original re-initialization equation and the accuracy of the constrained re-initialization scheme.

Another different re-initialization equation is proposed by Chang et al. [78], who performed the re-initialization procedure by solving a perturbed Hamilton-Jacobi equation

$$\frac{\partial\phi}{\partial\tau} + (A_0 - A(t))(-P + \kappa)|\nabla\phi| = 0 \quad (18)$$

to a steady state, where A_0 denotes the total mass at the initial condition, $A(t)$ denotes the total mass at time t , P is a positive constant. This formulation is based on the observation that numerical diffusion introduces a normal motion proportional to the local curvature [79]. The difference in the mass, $(A_0 - A(t))$, is of order $O(\Delta x^2)$ in the smooth region and it does not change the overall accuracy of the method.

For the hyperbolic tangent level set method, the corresponding re-initialization equation (Eq. (11)) is solved in various cases [64,65,68]. To some extent, this re-initialization equation is similar to the conservative equation in phase field method [80]. McCaslin and Desjardins [81] further improved the re-initialization equation to account for a significant amount of spatial variability in the level set transport. This local re-initialization is based on the estimation of local flow deformation and numerical diffusion. A spatially and temporally varying factor is introduced into the re-initialization equation to yield

$$\frac{\partial\psi}{\partial\tau} = \nabla \cdot \left(\alpha \left(\varepsilon (\nabla\psi \cdot \vec{n}) - \psi(1-\psi) \right) \vec{n} \right) \quad (19)$$

The local interfacial value of α is defined as

$$\alpha(\vec{x}_\Gamma, t) = \max \left(\lambda_n |\vec{u}_\Gamma \cdot \vec{n}|, \lambda_s |\vec{n}^T \cdot S_\Gamma \cdot \vec{n}| \varepsilon \right) \quad (20)$$

where $\lambda_n |\vec{u}_\Gamma \cdot \vec{n}|$ measures the numerical diffusion and $\lambda_s |\vec{n}^T \cdot S_\Gamma \cdot \vec{n}| \varepsilon$ measures the deformation of local flow kinematics. Compared with the standard global re-initialization, this method proves to be able to reduce both the conservation error and the overall

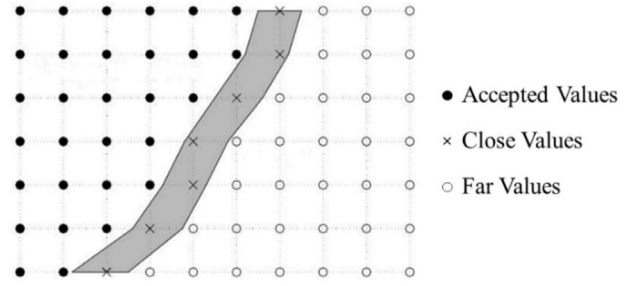


Fig. 8. Upwind construction of Accepted Values. Reprinted from Adalsteinsson and Sethian [61] with permission of Elsevier.

computational cost. For summary, the PDE based re-initialization equations used in the literature are listed in Table S2.

The FMM based re-initialization procedure was first proposed by Sethian [44]. In this framework, the FMM is efficiently used to solve the Eikonal equation for re-initialization $|\nabla\phi|=1$ by ordered sweeping in the direction of normal characteristics. Specifically, re-initialization of the signed distance function amounts to marching the front from the interface to the rest of the computational domain, as illustrated in Fig. 8. Crucial to the FMM process are the three lists A, C, and F, distinguishing each computational cell as “accepted”, “close”, and “far”, respectively. The upwind finite difference scheme is used to compute $\phi_{i,j,k}$ within each close cell in list C by solving the equation

$$\begin{aligned} & \max(D_x^- \phi_{i,j,k} - D_x^+ \phi_{i,j,k}, 0)^2 \\ & + \max(D_y^- \phi_{i,j,k} - D_y^+ \phi_{i,j,k}, 0)^2 \\ & + \max(D_z^- \phi_{i,j,k} - D_z^+ \phi_{i,j,k}, 0)^2 - 1 = 0 \end{aligned} \quad (21)$$

where $D_{x,y,z}^\pm$ are the first order upwind finite difference notations. Once ϕ has been computed in all close cells, it is added to list A and any of its adjacent far neighbors are removed from list F and added to list C. The process of solving Eq. (21) is repeated and the entire procedure is performed separately for regions corresponding to $\phi < 0$ and $\phi \geq 0$. This method benefits the re-initialization procedure in terms of computational cost, and can be straightforwardly extended to achieve higher-order accuracy [44,57,68].

In addition, some other re-initialization methods have also been proposed recently in the literature, such as the geometric mass-preserving re-distancing scheme [82] and the volume re-initialization scheme including the effect of local curvature [83].

2.2.6. Hybrid method

The level set method has also been coupled with other techniques to reduce the mass loss. Sussman et al. [84,85] firstly proposed a coupled level set/volume-of-fluid (CLSVOF) method, which takes advantages of the mass conservation property of the VOF method. In the CLSVOF method, after the advection step of the level set scalar and volume fraction scalar, the coupling between the two scalars occurs twice. The first coupling happens when the interface is reconstructed with the interface normal vector directly computed as $\vec{n} = \nabla\phi$. The second coupling occurs when ϕ is reinitialized to the signed distance from the reconstructed interface. This re-initialization to the signed distance is actually quite complicated since it is necessary to consider portions of the cell boundary in order to keep the level set scalar continuous, as shown in Fig. 9. As a consequence, many improvements on the CLSVOF method [86–91] have been made and other versions such as, the coupled volume-of-fluid and level set method [92], the conservation correction equation method [93], and the level set-volume constraint method [94] have been developed. But still, these coupled level set methods suffer from complexity

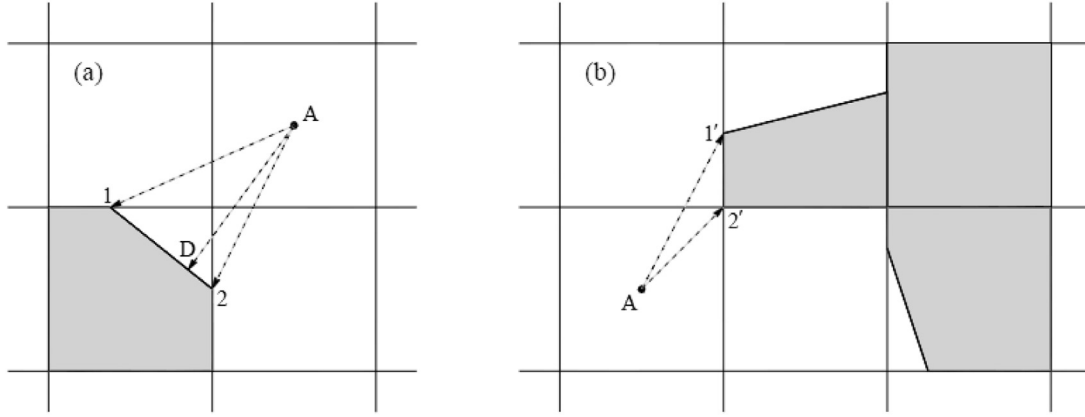


Fig. 9. The re-initialization to the signed distance from the interface segment 1–2. (a) The intersection point D is inside the segment; (b) The intersection point D is outside the segment. Reprinted from Tryggvason et al. [23] with permission of Cambridge University Press.

in implementation, including the advection of both the level set function and the volume fraction, the piecewise linear interface construction, and the subsequent reconstruction of level set scalar based on this piecewise linear interface as well as the coupling between scalars.

To reduce the complexity in implementation, Pijl et al. [95,96] proposed a coupled mass-conserving method, in which the level set and the volume fraction were used without the complicated interface constructions. This method is based on the level set method, using a VOF function to conserve mass. Crucial to this method is the relationship between the level set function ϕ and the volume of fluid function ϕ_{vol} . The volume of fluid function ϕ_{vol} is first computed from the level set function ϕ , and then advected conservatively. The level set function ϕ then can be easily updated by using the volume of fluid function ϕ_{vol} through a iteration procedure. This method has been improved by Luo et al. [97]. They further improved the mass conservation of the liquid phase by correcting the volume fraction based on the local curvature on the interface. This mass remedy procedure includes three steps as follows:

- 1) The relative volume of the liquid phase in a computational cell, i.e., the volume fraction $\phi_{vol}^{n+1,*}$, is computed from the level set function $\phi^{n+1,*}$;
- 2) The volume fraction $\phi_{vol}^{n+1,*}$ is corrected for mass conservation based on the curvature of each cell on the interface within a time step towards ϕ_{vol}^{n+1} ;
- 3) With the new volume fraction ϕ_{vol}^{n+1} , corrections to $\phi^{n+1,*}$ are obtained by solving $f(\phi^{n+1}, \nabla\phi^{n+1}) = \phi_{vol}^{n+1}$.

A similar method based on the sigmoid function can be found in Chai et al. [98].

Additionally, the particle level set method has been developed in order to combine the accuracy of the Lagrangian front tracking with simplicity and the efficiency of the level set method. In this method, the Lagrangian marker particles are passively advected with flow and are used to rebuild the level set function in under-resolved regions [99]. This is usually the case for flows undergoing stretching and tearing. Other improvements on the particle level set method can be found in [54,100–102]. Initially, the particles are set within a band across the interface. Each particle stores its position and radius that are used to perform the error correction to the level set. The particle radius can be expressed as,

$$r_p = \begin{cases} r_{\max}, & \text{if } s_p \phi(\vec{x}_p) > r_{\max} \\ s_p \phi(\vec{x}_p), & \text{if } r_{\min} \leq s_p \phi(\vec{x}_p) \leq r_{\max} \\ r_{\min}, & \text{if } s_p \phi(\vec{x}_p) < r_{\min} \end{cases} \quad (22)$$

where s_p is the sign of the particle that is set to +1 if $\phi(\vec{x}_p) > 0$ and -1 if $\phi(\vec{x}_p) < 0$, $r_{\min} = 0.1 \min(\Delta x, \Delta y, \Delta z)$ and $r_{\max} = 0.5 \max(\Delta x, \Delta y, \Delta z)$. Whenever a particle escapes from the interface by more than its radius, it will be used to perform the error correction on the interface. The particle predicted level set value for each corner of the cell containing the escaped particle is defined as

$$\phi_p(\vec{x}) = s_p(r_p - |\vec{x} - \vec{x}_p|) \quad (23)$$

For each positive escaped particle, ϕ_p is compared to the local value of ϕ and the maximum of these two values is taken as ϕ^+ . For each negative escaped particle, ϕ_p is compared to the local value of ϕ and the minimum of these two values is taken as ϕ^- . The level set is then reconstructed by choosing the value with minimum as

$$\phi = \begin{cases} \phi^+ \text{ if } |\phi^+| \leq |\phi^-| \\ \phi^- \text{ if } |\phi^+| > |\phi^-| \end{cases} \quad (24)$$

2.2.7. Variational level set method

In the basic level set formulation, the re-initialization process is obviously a disagreement between the theory and its implementation [103], and many developed re-initialization processes have undesirable side effects on the interface [104]. As a result, some efforts to attempt the level set method without re-initialization process have been made, such as the variational formulation [105,106], the modified level set equation [63], and the stabilized variational method [107].

In these methods, the level set function is defined on a domain, and the energy function is defined as

$$\Theta(\phi) = \alpha \int_{\Omega} I(|\nabla\phi|) d\mathbf{x} \quad (25)$$

where α is a constant and I is an energy density function. The minimization of the energy $\Theta(\phi)$ is to regulate the level set function as a signed distance function. Considering that the signed distance function satisfies the Eikonal equation $|\nabla\phi|=1$, one can simply define the energy density function as

$$I(|\nabla\phi|) = \frac{1}{2} (|\nabla\phi| - 1)^2 \quad (26)$$

Mathematically, a standard method to minimize the energy functional $\Theta(\phi)$ is to find the steady-state solution to the gradient flow equation

$$\frac{\partial\phi}{\partial t} = -\frac{\partial\Theta}{\partial\phi} \quad (27)$$

where $\partial\Theta/\partial\phi$ is the Gâteaux derivative of the function $\Theta(\phi)$.

By calculating the variations and recalling the motion of the level set function, the evolution equation of the level set function can be rewritten as

$$\frac{\partial \phi}{\partial t} + \vec{u} \cdot \nabla \phi = \alpha \cdot \operatorname{div} \left[\left(1 - \frac{1}{|\nabla \phi|} \right) \nabla \phi \right] \quad (28)$$

in which the factor $1 - 1/|\nabla \phi|$ can be regarded as the diffusion rate. If $|\nabla \phi| > 1$, the diffusive rate is positive and the diffusion is forward to decrease $|\nabla \phi|$; If $|\nabla \phi| < 1$, the diffusive rate is negative and the diffusion is backward to increase $|\nabla \phi|$. It should be noted that this diffusion has an undesirable side effect on the evolution of the level set function when $|\nabla \phi|$ is close to zero leading to an unbounded diffusion rate. This infinite diffusion rate will contaminate the accurate location of the zero level set, especially for the narrow-band level set function, which has been improved in [108].

It should be summarized here that the above seven types of strategies are all aiming at improving the mass-conservative property of the basic level set formulation. The former four categories are related to the first reason of mass loss while the others are related to the second reason. In particular, the former four categories focus on numerical measures, including using the high-order schemes, the extension velocity, the better level set function, and the locally refined grid, to improve the discretization, whereas the others consider variant level set method with alternative re-initialization or even without re-initialization process. It is expected that the interface refined level set method coupling with the VOF method is the most attracting and promising tool for simulations of atomization and evaporation. In this kind of coupled methods, however, the reconstruction procedures between the signed distance function and volume fraction are expected to induce errors on interface location that can deteriorate the curvature accuracy, leading to stability issues in configurations that involve high capillary numbers [68,109]. Indeed, if the interface normal and the curvature of Eq. (2) are calculated from a smoothed version of the sharp volume fraction rather than the signed distance function, spurious oscillations occur as reported in [68]. For years, this has been a strong advantage for the level set method since even methods with weak mass conservation properties such as the original formulation of Sussman et al. [43] can exhibit very good stability and accuracy properties in regard to the capillary force. As a result, there is currently not a general agreement on addressing the well-known mass conservation issue, and more efforts need to be made along this line.

3. Level set method for atomization with evaporation

With the development of computational capacity, the level set method has been widely used to directly simulate the atomization process [68,110,111]. In 2008, Gorokhovski and Herrmann [12] have outlined some severe numerical challenges that occur in interface-resolved modelling of primary atomization, and related numerical strategies to address them. The numerical issues are briefly summarized here as: length and time scales, interface topology changes, material property discontinuities, surface tension treatments and inherent 3D configurations. Some state-of-the-art strategies for surface tension treatment [112] and large density ratio treatment [113] have been accessible, we will not go into details here. In realistic spray combustion applications, however, the liquid evaporates simultaneously with the atomization process, which means the interaction between the atomization and evaporation should be considered for a better understanding of the physical processes. Consequently, challenges increase in detailed numerical simulations due to the heat and mass transfer as well as the generated Stefan flow near the interface. We will address these challenges in the context of the level set method in the present review.

3.1. Governing equations

For the Navier–Stokes equations of two-phase flows that involve variable discontinuities on the interface, there are three different formulations, namely the “Whole-Domain Formulation”, the “Whole-Domain Conservation Law Form” and the “Jump Condition Form” [114]. The former two forms express the discontinuities as singular source terms in the governing equations by introducing a Dirac distribution at the interface, whereas the third form separately solves the equations and imposes an additional jump condition on the interface to respect the discontinuities. These formulations are theoretically equivalent [115,116]. However, a main difficulty arises in accurately discretizing the singular source terms [117,118] for the former two forms. In contrast, the “Jump Condition Formulation” allows a sharper representation of the discontinuity terms [119]. As the evaporation rate is usually calculated from the jump conditions in the regions just adjacent to the interfaces, the governing equations for incompressible evaporating gas-liquid flows are expressed in the “Jump Condition Form” as

$$\nabla \cdot \vec{u} = 0 \quad (29)$$

$$\frac{\partial \rho \vec{u}}{\partial t} + \nabla \cdot (\rho \vec{u} \otimes \vec{u}) = -\nabla p + \nabla \cdot (\mu [\nabla \vec{u} + \nabla \vec{u}^t]) + \rho \vec{g} \quad (30)$$

where ρ is the density, \vec{u} is the velocity vector, p is the pressure, μ is the dynamic viscosity and \vec{g} is the gravitational acceleration.

Since evaporation and subsequent combustion processes need information of temperature and vapor mass fraction, the following temperature and species equations [118,119] should also be solved

$$\frac{\partial \rho C_p T}{\partial t} + \nabla \cdot (\rho C_p \vec{u} T) = \nabla \cdot (\lambda \nabla T) \quad (31)$$

$$\frac{\partial \rho Y}{\partial t} + \nabla \cdot (\rho \vec{u} Y) = \nabla \cdot (\rho D_m \nabla Y) \quad (32)$$

where T is the temperature, λ is the thermal conductivity, C_p is the specific heat at constant pressure, Y is the mass fraction, and D_m is the mass diffusion coefficient.

To fully respect the mass conservation, momentum conservation and energy conservation across the interface, additional jump conditions (or boundary conditions) should be provided on the interface. However, while benefiting much from the implicit definition of the convoluted interface, the level set method meets difficulties in imposing these jump conditions. In particular, they are not straightforwardly imposed on the interface but are in the adjacent cells instead [120]. As a result, the ghost fluid method (GFM) [121] has been incorporated, and the following sections discuss the specific numerical issues and treatments.

3.2. Numerical issues and treatments of atomization with evaporation

Except for those typical challenges addressed previously by Gorokhovski and Herrmann [12], the following issues are specifically appeared for evaporation simulations: (1) The evaporation process adds new jump conditions across the interface to the governing equations and further increases the complexity of system. (2) Unrealistic mass predictions may easily take place in the high density ratio case if the velocity field extension of the liquid phase cannot respect the divergence-free condition in the whole domain. (3) The general and effective method to determine the evaporation rate in different situations still remains the way ahead. These numerical issues and the state-of-the-art treatments for them will be presented as follows.

3.2.1. Interface jump conditions and their treatments

As aforementioned, the level set method essentially allows a sharp but implicit presentation of the interface. Therefore, imposing the jump conditions need careful treatments. The jump conditions across the interface can be classified into three categories: the material property jump condition, the zero-order jump condition, and the first-order jump condition. For convenience, three subscripts l , g and Γ are defined here to respectively indicate the liquid phase, the gas phase and the interface. A jump operator $[\cdot]$ across the interface Γ is also defined:

$$[A]_{\Gamma} = A_l - A_g \quad (33)$$

The material jump condition denotes the jumps of physical properties including the density ρ , the dynamic viscosity μ , the thermal conductivity λ and the specific heat C_p . When simulating incompressible two-phase flows, these physical properties are usually assumed to be constant in each phase, but jump on the gas-liquid interface as: $[\rho]_{\Gamma} = \rho_l - \rho_g$, $[\mu]_{\Gamma} = \mu_l - \mu_g$, $[\lambda]_{\Gamma} = \lambda_l - \lambda_g$, $[C_p]_{\Gamma} = C_{pl} - C_{pg}$. Note that the latter two terms are newly introduced by the energy and species equations.

The zero-order jump condition includes the jumps of the velocity and the pressure. Due to the Stefan flow near the interface, the velocity is no longer continuous across the interface. Applying the mass conservation across the interface [119,122], the relationship between the evaporation rate $\dot{\omega}$, i.e. the local evaporation mass flow rate per unit surface, and the velocity can be derived as

$$\dot{\omega} = \rho_l (\vec{u}_s - \vec{u}_l) \cdot \vec{n} = \rho_g (\vec{u}_s - \vec{u}_g) \cdot \vec{n} \quad (34)$$

where \vec{u}_s denotes the interface velocity, i.e. the sum of the liquid phase velocity \vec{u}_l and the interface regression speed $\dot{\omega} \vec{n} / \rho_l$ due to evaporation. As a result, the velocity jump condition across the interface can be expressed as

$$[\vec{u}]_{\Gamma} = -\dot{\omega} \left[\frac{1}{\rho} \right]_{\Gamma} \vec{n} \quad (35)$$

In some simple situations such as static liquid evaporation, one can set up a velocity potential to derive the velocity as did by Tangy et al. [119]. Similarly, the contribution of the recoiling pressure should be added to the pressure jump to account for the evaporation effects. The term accounting for the discontinuity of the viscous normal component should also be modified compared to that without phase change, as the velocity is no longer continuous across the interface. Consequently, the pressure jump condition across the interface reads as [123]

$$[p]_{\Gamma} = \sigma \kappa + 2[\mu \vec{n}^t \cdot \nabla \vec{u} \cdot \vec{n}]_{\Gamma} - \dot{\omega}^2 \left[\frac{1}{\rho} \right]_{\Gamma} \quad (36)$$

where σ is the surface tension coefficient.

The first-order jump condition refers to the Rankine-Hugoniot jump [124,125] across the interface to respect the energy conservation and the mass conservation:

$$h_{lg} \dot{\omega} - [\lambda \nabla T \cdot \vec{n}]_{\Gamma} = 0 \quad (37)$$

$$\omega Y_l^{\Gamma} + [\rho D_m \nabla Y \cdot \vec{n}]_{\Gamma} = \dot{\omega} Y_g^{\Gamma} \quad (38)$$

where h_{lg} is the latent heat of evaporation. The evaporation rate for sharp interface methods can be directly calculated from this kind of jump conditions in interface-resolved detailed numerical simulation.

Numerical difficulties arise in accurately imposing these jump conditions especially the Rankine-Hugoniot jumps for heat and mass transfers according to Tangy et al. [119]. In order to discretize the jump conditions sharply, instead of smearing out the discontinuous terms near the interface, the GFM [121] is utilized

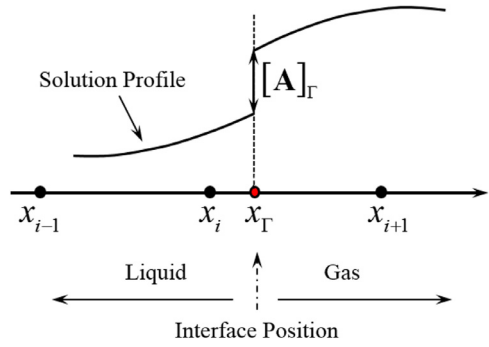


Fig. 10. Illustration of the GFM for a variable A which displays a discontinuity on the interface.

as a powerful technique, which has been applied to incompressible flow with phase change [117,126] and compressible reacting flows [127]. Fig. 10 illustrates the GFM for a variable A which displays a discontinuity on the interface. As expected, difference stencils for cell x_i will usually require the value at x_{i+1} , which is invalid for numerical discretization due to the discontinuity. Consequently, the GFM creates an artificial continuous profile that accounts for the jump conditions on the interface and provides a ghost value at x_{i+1} to keep the discretization uniform. While the level set method provides an implicit representation of the interface, the GFM allows an explicit representation of the interface jump conditions. Thus, the overall level set/GFM scheme is quite easy to implement in complex configurations.

In the framework of the level set/GFM combination, Liu et al. [128] have proposed a general method for enforcing interface jump conditions on irregular domains. The jump conditions were specified as a linear combination of the jump of a variable and the jump of its normal derivative. Special care was devoted to the treatment of the normal derivative jump, in which the normal derivative jump was rewritten as three separate terms corresponding to the coordinate directions. Although this division smears out the tangential derivatives, it correctly captures the jump in the normal derivative and allows one to deal with the jump conditions in a dimension by dimension fashion. This method is robust, easy to implement and symmetric, making the fast iterative solver workable for large-scale simulations. In the same framework, some state-of-the-art numerical methods have also been developed for the Dirichlet boundary conditions [124,129], the Neumann boundary conditions [130], the Robin boundary conditions [120,131], and the mixed boundary conditions [132]. Interested reader could refer to these references for more details.

During the procedure of imposing the jump conditions (or boundary conditions), the ghost values are required to keep the discretization uniform in the following situations:

- 1) As the interface moves, the grid cells swept by the interface at two consecutive time steps t^n and t^{n+1} may no longer have valid values for A due to the discontinuities. For example, the grid cell of the dark point with a question mark in Fig. 11.
- 2) Even for a still-interface case, the discretization stencil passes across the interface and extends to the other-side subdomain where no valid values exist.

A popular approach to provide such ghost values is using an extrapolation method to extend A from its known subdomain to the unknown one. In particular, Aslam [134] proposed a general way for multidimensional extrapolation. Arbitrary orders of polynomial extrapolation can be formulated in this approach by simply solving a series of linear partial differential equations (PDEs). Recently, McCaslin et al. [135] have proposed a fast marching approach to the multidimensional extrapolation. Instead of converging the

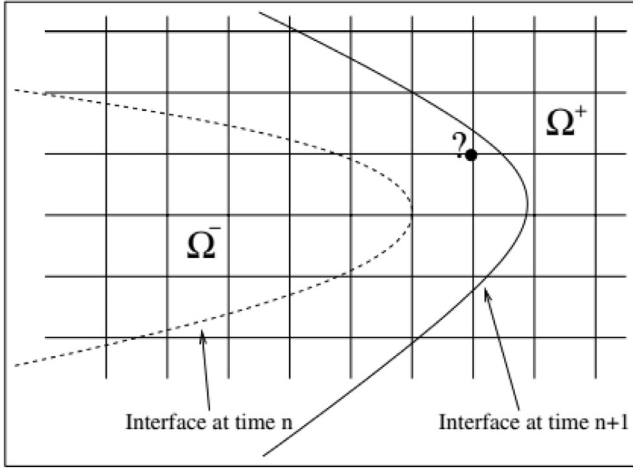


Fig. 11. Interface at two consecutive time steps t^n (dashed line) and t^{n+1} (solid line). Reprinted from Gibou et al. [133] with permission of Elsevier.

PDEs to steady state, this approach solves the non-homogeneous Hamilton–Jacobi equations, which are mathematically identical to the steady-state PDEs, by using the FMM. Results showed that the FMM extrapolation method reduces the computational cost compared to the PDE extrapolation method. More details on the mathematical formulations of these two extrapolations can be found in [Appendix A](#).

Actually, since only a narrow band close to the interface needs ghost values for the GFM, one does not really need to solve the PDEs to steady state in the whole domain, but can advance them only in a few steps in the narrow band region. As a result, the computational cost of the PDE extrapolation remains acceptable. Furthermore, the directional derivatives of T and Y in the normal direction can be used conveniently to calculate the evaporation rate.

3.2.2. Navier–Stokes equations and divergence-free velocity extension

The projection method [136] is an advantageous tool for discretizing the incompressible Navier–Stokes equations because the velocity and the pressure fields are decoupled. This method consists of three steps: (1) obtain an intermediate velocity field at a new time step $n+1$ by advancing the momentum equation without pressure term; (2) calculate the pressure through the pressure Poisson equation; and (3) correct the velocity field to ensure continuity using the pressure gradient.

In simulations of evaporating two-phase flows, however, the velocity becomes no longer continuous across the interface due to the Stefan flow. When the GFM formula is used to address the velocity jump during the above prejection steps, extending the ghost velocities from liquid/gas phase to gas/liquid phase is necessary. Nguyen et al. [122] once proposed such an extension method for reactive interface, and the ghost velocities were simply evaluated from [Eq. \(35\)](#) as

$$\vec{u}_l^{ghost} = \vec{u}_g - \dot{\omega} \left[\frac{1}{\rho} \right]_{\Gamma} \vec{n} \quad \text{and} \quad \vec{u}_g^{ghost} = \vec{u}_l + \dot{\omega} \left[\frac{1}{\rho} \right]_{\Gamma} \vec{n} \quad (39)$$

However, this extension may lead to unrealistic mass predictions for liquid–gas interface with high density ratio, as pointed out by Tanguy et al. [119]. In particular, they addressed that the liquid phase velocity extension is not fully satisfactory because the extension does not respect the divergence-free condition in the whole domain. To solve this problem, they presented an improvement of the liquid velocity field extension to preserve the divergence-free condition on the interface. The detailed description can be found in [Appendix B](#). This improved velocity exten-

sion has been validated by a theoretical test, in which a droplet is upward pushed due to the generated Stefan flow in a top-opened container [119], and applied to many problems such as [117,137].

Recently, Lee et al. [138] have also presented an improved approach to reduce the numerical oscillations, spurious currents and mass flux errors. The approach features a diffused interface and a post-advection velocity correction to ensure accurate velocity divergence in the interfacial cells. In particular, the correction updates the original velocity field twice to satisfy the divergence-free condition prior to the standard projection method. This treatment can help mitigate the spurious pressure fluctuations by maintaining consistency between density and velocity jumps at all times.

3.2.3. Calculation of evaporation rate

The evaporation models based on the point-source assumption have been extensively used to determine droplet evaporation rate in the past two decades [3]. Realistic liquid topologies, however, will inevitably violate the assumption because of deformation and internal circulation. Recent interface-resolved DNS methods are able to calculate the evaporation rate directly from the first-order jump conditions, and can deal with evaporation on irregular evolving interfaces. We refer to the method that calculates $\dot{\omega}$ from the temperature jump condition as the Heat Flux based Model (HFM) and that from the species concentration jump condition as the Species Mass Flux based Model (SMFM), respectively. For convenience, only mono-component liquid phase is considered in this section. When the liquid is multi-component [139], the calculation of the evaporation rate will be slightly more complicated.

The HFM for evaporation relies on a basic assumption that the interface temperature has already reached the steady state saturation temperature T_{sat} , which for example is the wet bulb temperature or the boiling temperature. The value of T_{sat} can be estimated via a psychrometric chart and/or empirical correlations [140]. According to this assumption, the evaporation rate is totally driven by the net conductive heat flux density. As a result, the temperature equation [Eq. \(31\)](#) can be solved separately in the liquid and gas subdomains with a Dirichlet boundary condition $T_l^\Gamma = T_g^\Gamma = T^\Gamma$ on the interface. Note that a saturation temperature difference exists due to the pressure jump across the interface, leading to a question of what value should be chosen for T^Γ . The detailed discussion on how to determine T^Γ can be found in [Appendix C](#). Once the temperature field is solved, [Eq. \(37\)](#) is available to evaluate the evaporation rate $\dot{\omega}$, making it consistent with the net heat flux on the interface:

$$\dot{\omega} = [\lambda \nabla T \cdot \vec{n}]_\Gamma / h_{lg} \quad (40)$$

In particular, when more heat flows into the interface than flows out, the heat will be absorbed by the liquid just near the interface, leading to liquid evaporation. When more heat flows out than flows in, a condensation process happens.

In contrast, the SMFM for evaporation does not use any restrictive assumptions. It is suitable for more general situations because the species gradient, which is the driving force for evaporation in this model, can interact with the temperature field. In the case of mono-component liquid, the mass fraction Y is of interest only in the gas phase. That is, the species equation of [Eq. \(32\)](#) can be solved only in the gas phase with a Dirichlet boundary condition for the vapor concentration on the interface Y_{vap}^Γ . The vapor pressure on the interface is expected to be the saturation pressure p_{vap}^Γ , which and Y_{vap}^Γ can be given by the Clausius–Clapeyron relation as:

$$p_{vap}^\Gamma = p_{atm} \exp \left(- \frac{h_{lg} m_{vap}}{R} \left(\frac{1}{T^\Gamma} - \frac{1}{T_B} \right) \right) \quad (41)$$

$$Y_{vap}^{\Gamma} = \frac{p_{vap}^{\Gamma} m_{vap}}{(p_{atm} - p_{vap}^{\Gamma}) m_g + p_{vap}^{\Gamma} m_{vap}} \quad (42)$$

where p_{atm} is the ambient pressure, m_{vap} is the molar mass of the vapor, R is the perfect gas constant, T_B is the liquid boiling temperature for the ambient pressure and m_g is the molar mass of the ambient gas. Eq. (38) is now available to evaluate the evaporation rate $\dot{\omega}$ while Eq. (37) imposes the necessary condition for the temperature field. Because the gradient of the mass fraction is zero in the liquid phase, $\dot{\omega}$ is derived from Eq. (38) as

$$\dot{\omega} = \frac{\rho_g D_m \nabla Y \cdot \vec{n}|_{\Gamma}}{1 - Y_{vap}^{\Gamma}} \quad (43)$$

Comparatively, the HFM considers that the interface temperature is equal to the saturation temperature, whereas the SMFM allows variations of interface temperature in regards to the chemical composition of the gas phase on the interface. As a consequence, the HFM is limited to phase change computations of a single component liquid with its vapor (boiling) in the literature, whereas the SMFM is applicable to accounting for two chemical species in the gas phase (droplet evaporation in an inert gas for instance). It is noteworthy, however, that the HFM can also handle droplet evaporation in ambient gas phase under certain circumstances when the interface temperature has reached a steady state condition (the wet temperature for instance). In this case, providing a species solver for the HFM is of interest [141,142].

Despite of its generality in application, the sequential calculation procedure of the SMFM is fragile and unstable for high evaporation flux cases. In such situations the denominator in Eq. (43), i.e. $1 - Y_{vap}^{\Gamma}$, approaches zero, which significantly amplifies the small errors near the interface. To reduce the errors, smaller time step is usually required, making the computational cost increases exponentially [141]. Son [143] tried to address this issue by using a Newton-Raphson iterative algorithm to restrict the interface temperature and therefore obtain a sufficiently large denominator. However, this modification was not physically correct because the modified interface temperature could not approach the boiling temperature.

As introduced above, the HFM and SMFM each exhibit strengths and shortcomings. Recently, Villegas et al. [137] have combined the HFM and SMFM to develop an improved effective method for calculating the evaporation rate. Specifically, the species equation of Eq. (32) is solved with a prescribed Robin boundary condition on the interface, which is derived from Eq. (38) as following:

$$\dot{\omega} Y_{vap}^{\Gamma} + \rho_g D_m \vec{n} \cdot \nabla Y|_{\Gamma} = \dot{\omega} \quad (44)$$

where $\dot{\omega}$ is calculated from Eq. (37) based on the heat flux across the interface. Once the species equation is solved, the non-homogeneous interface temperature can be determined by reversing the Clausius-Clapeyron relation of Eqs. (41) and (42):

$$T^{\Gamma} = \frac{h_{lg} m_{vap} T_B}{h_{lg} m_{vap} - RT_B \ln \left(\frac{p_{vap}^{\Gamma}}{p_{atm}} \right)} \quad (45)$$

where p_{vap}^{Γ} is determined as

$$p_{vap}^{\Gamma} = \frac{-Y_{vap}^{\Gamma} p_{atm} m_g}{(m_g - m_{vap}) Y_{vap}^{\Gamma} - m_{vap}} \quad (46)$$

Hence, the temperature equation can be solved with a non-homogeneous Dirichlet boundary condition. In this hybrid approach, the same set of equations are solved as those of the SMFM, while the overall algorithm has been reversed. Unlike the SMFM, this approach is stable even if the gas phase is saturated of vapor. As such, this approach can handle both evaporation and boiling depending on the external condition without requiring any sensors.

To summarize, this section concerns recent progress in DNS of evaporating two-phase flows using the level set method. Numerical obstacles introduced by the evaporation process are discussed, which stem from the potential for unphysical pressure oscillations, spurious velocity fields and mass flux errors across the interface. The well-established treatments are also presented. Recently, the interface-resolved method has been further extended to couple evaporation with combustion. Shao et al. [142] firstly incorporated droplet combustion with the level set method and succeeded in simulating the single *n*-heptane droplet and binary-droplet combustion process. Irfan and Muradoglu [145] successfully coupled detailed combustion mechanism with the front tracking method to simulate the falling droplet combustion. These advanced methods offer the potential to really study the underlying physics of spray combustion.

4. Application of the level set method to atomization and evaporation

With the development of the level set method and the computational capacity, the detailed numerical simulation of atomization and evaporation has drawn considerable attention. In the section, we give an overview on simulations of atomization and evaporation with the level set method, including the primary atomization, the secondary atomization, and the interfaces with evaporation. The relevant mechanisms and model developments are also discussed.

4.1. Primary atomization

In the recent years, there have been a lot of efforts to investigate the primary atomization. The typical numerical results from the recent ten-year studies are summarized in Fig. 12 and Table S3. For completeness, we include some results by using other interface tracking methods. Here we display four types of atomization, namely, straight jet, crossflow jet, impinging jet and swirling jet. These four types of atomization are usually related to diesel engine, gas turbines, rocket engine, and aircraft engine, respectively. Straight jet stands for the liquid jet injecting into still gas or the liquid jet surrounded by a coaxial flow of gas. Crossflow jet refers to the liquid jet injected into a gaseous crossflow. Impinging jet stands for the collision between two cylindrical liquid jets, and swirling jet refers to the liquid jet that has azimuthal swirl.

For the straight jet simulations, Kim et al. [146,147] investigated the primary breakup of a liquid round jet by a coaxial flow of gas by using the RLSG method [72] coupled with a Lagrangian spray model. The density ratio of the liquid and gas is 5. The Reynolds and Weber numbers of the liquid are 295 and 0.6 respectively. The Reynolds and Weber numbers of the gas based on the gas thickness are 3770 and 34 respectively. The numerical result of the interface is qualitatively well matched with the experimental observation by Marmottant and Villermaux [148], as illustrated in Fig. 12(d). It shows that the Kelvin-Helmholtz (KH) instability, producing axial perturbation, and the Rayleigh-Taylor (RT) instability, producing azimuthal perturbation, contribute to the formation of ligaments both in the experiment and the simulation. Indeed, the KH instability refers to an interfacial instability caused by shear between the slow fluid stream and the fast fluid stream while the RT instability occurs when the interface between two fluids of different densities experiences a pressure gradient opposing the density gradient.

By using the RLSG method, Herrmann took great efforts [72,149–151] to simulate the atomization process in its entirety with large range of length scales, which is shown in Fig. 12(e). The straight liquid jet into stagnant dense air under diesel engine conditions was investigated in [151], in which the density ratio of the

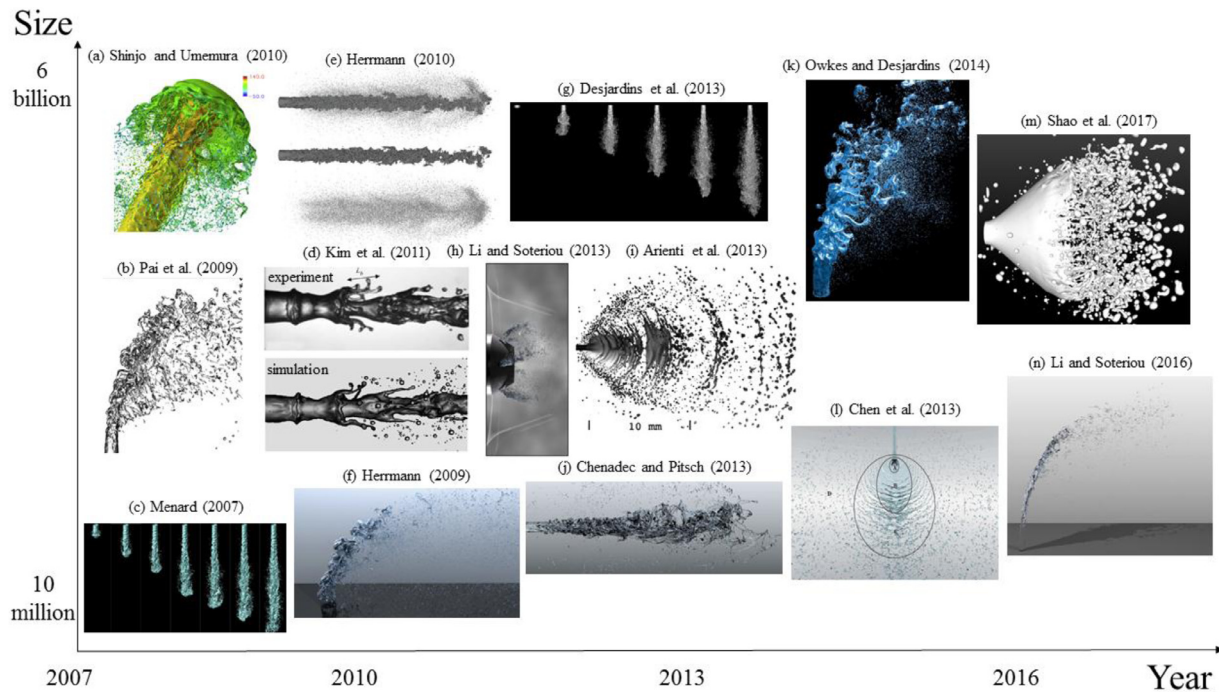


Fig. 12. State of the art for interface-resolved simulations of liquid atomization.

liquid and gas is 34, the viscosity ratio is 100, the Reynolds number is 5000, and the Weber number is 17,000. It was found that the turbulence is the driving mechanism or at least initiator of atomization within the first 20 diameters downstream of the injector. The drop size distribution is remarkably dependent on the grid resolution, and approaches the log normal distribution with increasing the grid resolution, which confirms that the grid independence test must be carefully conducted for atomization simulations [12].

Shinjo and Umemura [152] also made an intensive study of the straight primary atomization of liquid injected at high speed into still air as shown in Fig. 12(a). The level set method and the Multi-interface Advection and Reconstruction Solver (MARS) method were used. The Reynolds number is located in the range of 440–1470 and the Weber number is in the range of 1270–14,100. It is quite impressive that the total number of grid points in the largest case reaches six billion and the grid resolution is $0.35\text{ }\mu\text{m}$ to resolve the small droplet. A series of physical processes have been observed, including ligament formation, development of surface instability and droplet formation. The ligament formation is triggered by the liquid jet tip roll-up when the local gas Weber number is $O(1)$, and later ligaments are produced from the disturbed liquid core surface in the upstream. The disturbances are fed from the liquid jet tip toward upstream by vortices and droplet re-collision. The dominant mode is the short-wave mode driven by propagative capillary wave from the ligament tip, and the long-wave (Rayleigh) mode is not seen due to the absent injection nozzle. The liquid jet tip effects were further identified in [153]. The liquid jet front umbrella formation, atomization at the umbrella edge, mixing in the recirculation flow region and droplet generation mode were demonstrated in detail. The mechanism of liquid core surface instability was later investigated in [154] and it was suggested that the dominant mechanism could be the Tollmien-Schlichting (TS) instability in the parameter range of the study.

Desjardins and Co-authors [68,155] simulated the turbulent straight primary atomization by using a conservative level set/ghost fluid method, as shown in Fig. 12(g). The density ratio and viscosity ratio are 40. The Reynolds and Weber numbers are 3000 and 10,000, respectively. The inflow conditions were obtained

by simulating a turbulent pipe. The results showed that the liquid core has fully disintegrated by the end of the computational domain. The spectrally refined interface approach with sub-grid resolution was also applied to the simulation of turbulent liquid jets in quiescent air in [156]. The density ratio and viscosity ratio are 40. The Reynolds number is located in the range of 2000–3000 and the Weber number is in the range of 500–2000. It was demonstrated that the early interface deformation is caused by turbulent eddies that carry sufficient kinetic energy to overcome surface tension forces, which is consistent with the conclusion of [6,7], and the aerodynamics effects play an important role in the turbulent atomization of liquid jets. Effects of Weber number and Reynolds number were studied and detailed structures, such as, ligament rupture, bubble entrapment and drop splashing were observed. An air pocket in the liquid formed when the interface was pinched between two counter-rotating vortices. Recently, McCaslin and Desjardins [157] investigated the primary air-blast atomization of a planar liquid shear and modal analysis of flow instabilities has been conducted, demonstrating the streamwise growth of the shear layer and decay of the transverse vorticity.

Ménard et al. [88] investigated the primary straight atomization by the coupled level set/VOF/ghost fluid method, as shown in Fig. 12(c). The density ratio is 28 and the viscosity ratio is 120. The turbulent intensity of the inflow is 0.05. The Reynolds and Weber numbers are 5800 and 11,600, respectively. It showed that the 3D waves on the jet interface occur very closely to the jet exit. These surface instabilities are of great importance in the liquid atomization. Based on the DNS database, the Eulerian-Lagrangian Spray Atomization (ELSA) model was further evaluated in [158] and improved in [159]. By using the same method, Cousin et al. [160] performed the simulation of primary atomization of a liquid jet discharged by a low-pressure compound nozzle. The results with the internal inflow condition agreed well with the experiment. The liquid jet angle and the characteristic length scale of the perturbation were also well predicted quantitatively. Arienti and Sussman [161] performed the sharp-interface simulation of Diesel injector by using the CLSVOF method. The mean and root mean square (rms) values of axial velocity compared favorably with the exper-

iment. Other efforts to simulate the straight jet include the work by Chenadec and Pitsch [162] (shown in Fig. 12(j)) and the work by Tomar et al. [163].

Through simulations of straight jet by using the level set method, the correlation between liquid breakup and vortex dynamics has been investigated systematically [164–167]. The density ratio is in the range of 1.11–20. The viscosity ratio is in the range of 29–455. The Reynolds number is in the range of 320–5000. The Weber number is 230,000. It has been demonstrated that the counter-rotating, streamwise vortices around ligaments contribute to the instability behavior for jets flowing into like-density fluid in [164,165]. This implies that the density difference cannot fully explain the azimuthal instability observed by Marmottant and Villermaux [148] and Kim et al. [146,147]. The hole formation was found to be correlated with the hairpin and helical vortices, and dominated by inertial forces rather than capillary force, which differs from previous studies [152,156]. In addition, by investigating planar liquid jet, Zandian et al. [166] distinguished three atomization cascades based on the gas Weber number We_g and the liquid Reynolds number Re_l , i.e., lobe stretching at low Re_l and low We_g , bridge formation at moderate Re_l and high We_g , lobe corrugation at high Re_l and low We_g . These three distinct mechanisms have also been analysed in [167]. It shows that the interaction between the hairpins and KH roller explains the performance of the lobes, and the formation of the lobes is attributed to the streamwise overlapping of two oppositely oriented hairpin vortices on each side of the lobe.

To examine the above relevant studies in the Re - Oh space, it turns out that most of the straight jet simulations belong to the regime of the second wind induced breakup, as shown in Fig. 13. Only little work [164–167] belongs to the atomization regime. Studies over other regimes are required in future to give a full map of the problem.

For the crossflow jet simulations, Herrmann [168,169] performed detailed simulations of primary atomization of a turbulent liquid jet injected into a subsonic gaseous crossflow, which was analyzed experimentally [170], by using the RLSG method, as shown in Fig. 12(f). The density ratio is 10 and the viscosity ratio is 6. The jet Reynolds and Weber numbers are 14,079 and 2178, respectively. The crossflow Reynolds and Weber numbers are 570,000 and 330, respectively. The results indicated that breakup of the liquid jet occurs due to two main mechanisms. In the first mode, the insta-

bility waves on the liquid column generate role-ups and continue to grow along the jet axis until baglike structures form, which is attributed to the KH instability. Note that this mechanism for surface waves is contrary to the results conducted by Xiao et al. [8,9]. In the second mode, the corrugations on the liquid jet surface are stretched out into the ligaments at the sides of the jet near the injector exit, which is attributed to the RT instability. In addition, the smaller drops show a strong grid dependency, whereas the larger drops collapse to a log-normal distribution. By using the same configurations, the impact of density ratio on the liquid core dynamics was further studied [171,172]. It was shown that the increase in density ratio causes a noticeable increase in liquid core penetration and results in a decrease in the wavelength of the most dominant feature.

Behzad et al. [173] recently investigated a non-turbulent liquid jet injected transversely into a high pressure gaseous crossflow by using the level set method. The density ratio is in the range of 2–50 and the viscosity ratio is in the range of 2–10. The crossflow Reynolds number is in the range of 600–1200 and the crossflow Weber number is in the range of 60–96. The existence of shear instability on the jet periphery was identified as the primary destabilization mechanism. The temporal growth of such azimuthal instabilities leads to the formation of interface corrugations, which are eventually sheared off of the jet surface as sheet-like structures. The proposed instability mechanism is inherently an inviscid mechanism, contrary to the boundary layer stripping mechanism that is relied on a viscous interpretation. Behzad et al. [174] also performed temporal linear stability analysis of a jet in crossflow, and found the stability characteristics of the most amplified modes obtained from the numerical simulations are in good agreement with those of the stability analysis.

Owkes and Desjardins [175] conducted simulations of the atomization of a liquid jet in crossflow by using a conservative level set method, as shown in Fig. 12(k). The density ratio is 137 and the momentum flux ratio is 10. The liquid Reynolds and Weber numbers are 5430 and 5000, respectively. The gas Reynolds and Weber numbers are 9490 and 500, respectively. The effects of the round-edged and the sharp-edged injectors have been investigated and the results show that the sharp-edged injector which produces turbulent inflow significantly enhances the atomization process. The jet penetration, droplet size and velocity distributions were consistent with the experimental results. Pai et al. [110,176] investigated the effects of Weber numbers of the crossflow on the liquid primary atomization, as shown in Fig. 12(b). The crossflow Weber number is in the range of 500~3000. By using parametric study, it was found that the crossflow Weber number controls the characteristic thickness of the liquid structures, while the liquid Weber number controls the shapes of the liquid structures, such as blobs, tubes or sheets.

Li and Soteriou [177] simulated the liquid jet atomization in a gaseous crossflow with intermediate Weber numbers. The crossflow Weber number is in the range of 10–160 and the crossflow Reynolds number is in the range of 1391–5562. The liquid Reynolds number is in the range of 7896–31,583. The simulation was able to reproduce the experimentally obtained downstream droplet volumetric flux which exhibits a horseshoe shape, as shown in Fig. 12(n). The major findings include: (1) Formation of “ Λ ” shape windward waves was observed and explained by the combined upward and lateral surface motion. (2) The existence of RT instability as the primary mechanism for the windward waves was verified. (3) A peculiar “three - streak - two - membrane” liquid structure was identified at the lowest Weber number and explained as the consequence of the symmetric recirculation zones behind the jet column. Li et al. [178] further conducted simulations of atomization and evaporation in a liquid jet in crossflow for a realistic purpose by coupling with the evaporation model. It

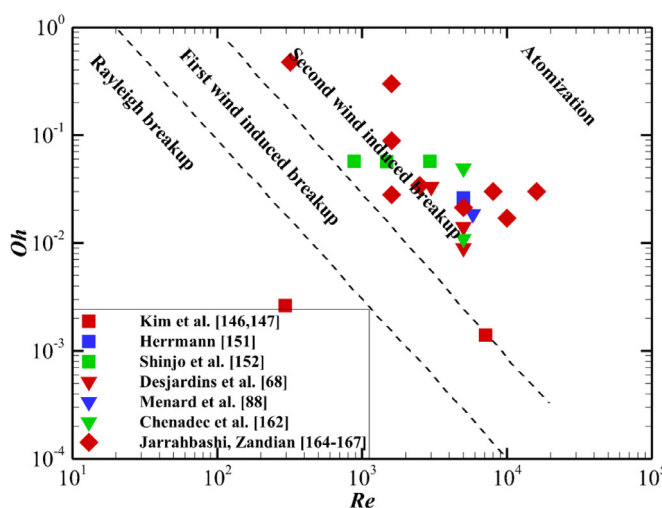


Fig. 13. Regimes of breakup for straight jet in Re - Oh space (Re is based on liquid jet).

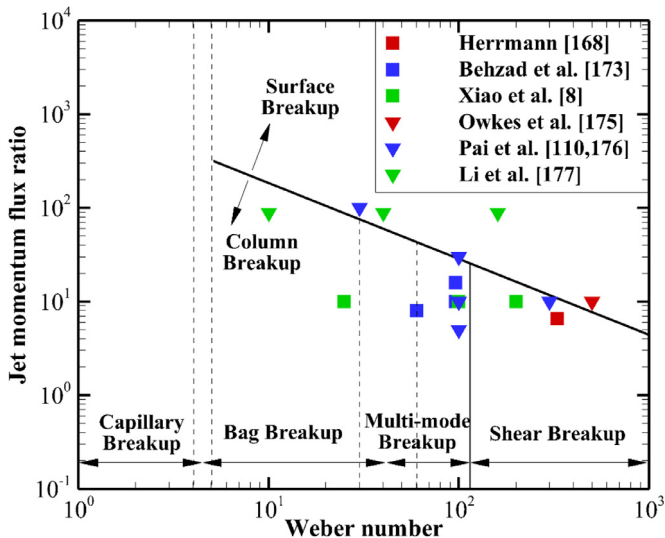


Fig. 14. Regimes of breakup for crossflow jet in $We-q$ space (We is based on crossflow.).

was found that when the injected liquid is at the same temperature as the crossflow gas, the vapor distribution is similar to that of the droplets. When the injected liquid is colder than the crossflow gas, the vapor distribution is center peaked.

When summarizing the above studies in the regime map of breakup in the $We-q$ space, it is found that most of the crossflow jet studies belong to the regime of column breakup, as shown in Fig. 14. It would be interesting to explore the breakup characteristics in other regimes in the future studies.

For the impinging jet simulations, Arienti et al. [179] performed a simulation of primary atomization by using the CLSVOF method with an adaptive mesh refinement (AMR) technique, as shown in Fig. 12(i). The density ratio is 832 and the viscosity ratio is 50. The Reynolds number in the pipe ranges from 4000 to 12,000. The linear instability analysis suggested that the KH instability may be at the base of ligament formation. Chen et al. [180] and Ma et al. [181] explored detailed flow physics associated with the temporal evolution and spatial development of a impinging jet over a wide range of Reynolds (40.4–11,724) and Weber numbers (27.5–2987), as shown in Fig. 12(l). Five flow patterns were reproduced, namely, liquid chain, closed rim, open rim, unstable rim and impact wave. As for the impact wave pattern, the entire flow evolution can be divided into four regions: the jet impingement, the flapping sheet, the ligaments, and the droplets. It was also found that the mean velocity profile has a profound effect on the stability characteristics.

The swirling jet is significantly important when applied to gas turbine combustors as an approach to enhance fuel-air mixing and flame stabilization. For numerical simulations, Li and Soteriou [182,183] simulated a realistic injector. The density ratio is 650 and the viscosity ratio is 83. The momentum flux ratio is 9.4 and the gas Weber number is 155. The qualitative feature of the flow is described, as shown in Fig. 12(h), and the results are contrasted against experiment data, providing a qualitative validation. Fuster et al. [184] also conducted numerical simulations of a swirling liquid flow with an emphasis on the potential of the code so that only mesh size test and drop size distribution were presented. Recently, Shao et al. [111] have performed detailed numerical simulations of a swirling liquid jet by using a conservative level set method with the maximum number of grids of about one billion, as shown in Fig. 12(m). The density is 20 and the viscosity ratio is 10. The Reynolds and Weber numbers are 2000 and 222, respec-

tively. The numerical results showed that turbulent inflow can induce liquid sheet breakup near the nozzle exit, reduce the stiffness of the liquid sheet, and lead to the statistically homogeneous distribution of small-scale liquid structures in the radial direction. The fluctuating velocity in the recirculation zone is statistically similar to isotropic turbulent and the liquid sheet can generate high shear layers to produce anisotropic small-scale fluctuations. Shao et al. [185] further investigated the detailed sheet, ligament and droplet formation in the swirling primary atomization. In general, the numerical results agreed well with experimental observations. The surface tension, pressure difference and swirling effect were found to contribute to the contraction and extension of the liquid sheet, and the ligament formation is partially attributed to the extension of the liquid hole. It is interesting to note that the movement of hairpin vortex exerts an anti-radial direction force on the sheet surface and leads to a sheet thinness, which is similar to the study of Jarrahbashi et al. [165] for straight jet.

In summary, detailed numerical simulations with the level set method have been extensively applied to primary atomization and are able to reproduce experimental obvervastions, even provide much more abundant information than experimental measurements. This offers an efficient way to understand various primary atomization in detail. However, the current simulation conditions are far from the experimental conditions of realistic applications. With increasing Reynolds number and Weber number to approach realistic experimental conditions, the computational cost will be extremely high even prohibitive. The obtained mechanisms of liquid primary breakup are different or contrary even in similar conditions, and the unified mechanism is still on the way ahead. In addition, the size distribution of small liquid structures in the atomization process is of particular importance. Some simulation results indicated that the drop size distribution in atomization obeys the log-normal distribution [152,169]. However, a log-normal distribution cannot be obtained unless the probability of breakup is independent of the particle size according to Epstein [186]. But in fact the breakup probability is proportional to second or third power of the particle size. This inconsistency of theory and numerical results needs further investigations.

4.2. Secondary atomization

The secondary atomization is the process of breakup of drops or ligament structures into smaller droplets. It usually involves in complex phenomena, such as, single droplet deformation and breakup, droplet collision, droplet impact on surface. Although some models have been developed to describe the secondary atomization process, for instance, the Taylor analogy breakup (TAB) model and the wave model, these models are not universal, with limited accuracy. This is partially due to the fact that the influencing factor and control mechanism of the secondary atomization have not yet been fully understood so that the assumptions based on which these models were established are suspicious. As a result, the level set method has also been extensively applied to investigate the mechanism of secondary atomization.

4.2.1. Single droplet deformation and breakup

There are two major concerns to investigate the single droplet deformation and breakup. One is the mechanism of secondary breakup, and the other is the drag coefficient of the deformable droplet.

Identifying various breakup modes for droplet fragmentation is the basic step to analyze the mechanism of breakup. Fig. 15 shows different breakup modes identified by previous studies in Oh_d - We_d space [187]. Here Oh_d is the droplet Ohnesorge number defined as $Oh_d = \mu_d / \sqrt{\rho_d \sigma D_d}$. We_d is the droplet Weber number defined as $We_d = \rho_g U_r^2 D_d / \sigma$, where U_r is the relative velocity between droplet

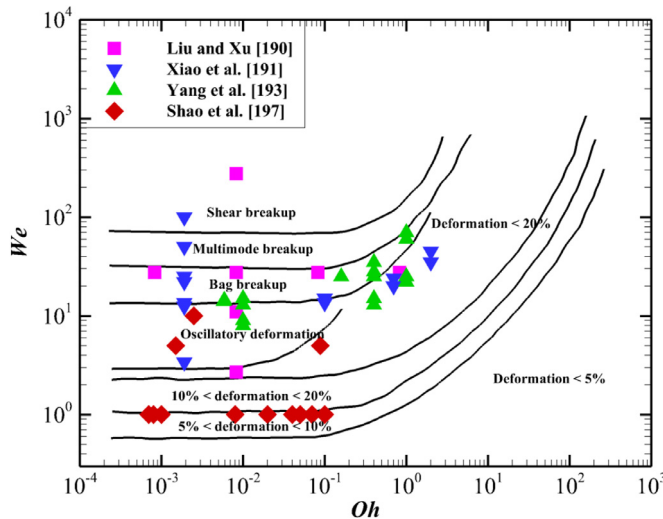


Fig. 15. Regimes of breakup in Oh - We space.

and gas flow. It is observed that the breakup modes can be classified in terms of the droplet Weber number for the Newton fluid in which the droplet Ohnesorge number is roughly less than 0.1. As non-Newton fluid is beyond the scope of the present review, the following studies mainly lie in the low droplet Ohnesorge number regimes.

Early studies on the droplet deformation and breakup are basically in two dimensional configurations. Balabel et al. [188] used the level set method to simulate oscillation and deformation of an initially elongated droplet in a quiescent fluid under the surface tension effect. The predicted oscillation process agrees well with that from the linear theory. Using a mass conserving level set method, Ni et al. [189] studied the effect of a wall on the droplet motion by setting a circular droplet between parallel walls and it was demonstrated that the Karman vortex street can explain the oscillatory mechanism of the falling droplet. For two or three droplets, the competition between wall repulsion and inter-droplet repulsion decides the droplet movement. Liu and Xu [190] used the classical level set method to simulate the droplet deformation and breakup in a two-dimensional gas flow. Four typical breakup modes, namely, oscillation, bag breakup, sheet stripping breakup, and shear breakup were observed. It was found that the gas Weber number is of the most importance to distinguish different breakup modes. In addition, multimode breakup containing shearing breakup and piercing breakup occurs when increasing the density ratio up to 1000.

Most of the above studies mainly handle two-dimensional, low-density ratio, and low Weber number conditions, which are believed to be limited by numerical algorithms and computational capacity. However, the actual secondary atomization process is usually three-dimensional and cannot be treated as axisymmetric deformation and breakup. Hence, three-dimensional simulation is imperative.

Xiao et al. [191] performed three-dimensional simulations of drop deformation and breakup at high density ratio of order $O(1000)$ by using the CLSVOF method. It was found that the RT instability dominates the drop breakup in the Weber number range of 3.4 to 96. The critical Weber number separating deformation and breakup regimes is also in good agreement with the experimental data. Xiao et al. [192] also performed simulations of drop deformation and breakup at different Weber numbers in supersonic flow. The bag breakup, bag stamen breakup and multimode breakup modes were reproduced and the RT instability was also found to determine the breakup morphology for the studied Weber

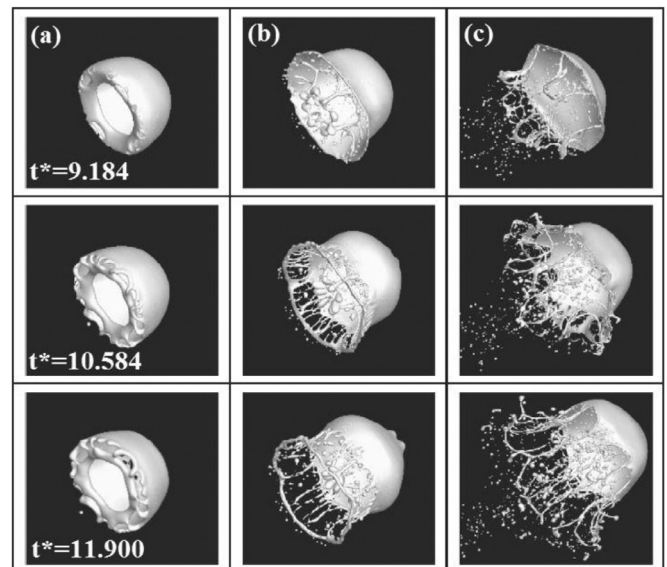


Fig. 16. Time resolved breakup process of a liquid droplet for $We_d = 225$, $Re_d = 10,062.5$: (a) $\rho^* = 10$, (b) $\rho^* = 25$, (c) $\rho^* = 60$, where t^* is the non-dimensional time. Reprinted from Yang et al. [194] with permission of Elsevier.

number ranges. Yang et al. [193] investigated transitions of deformation to bag breakup and bag to bag-stamen breakup for droplets subjected to gas flow by using the CLSVOF method. It indicated that the breakup modes in the bag-type regimes are determined by the ratio of droplet diameter to the wavelength of the most unstable RT wave. By using the same method, Yang et al. [194] further investigated the influence of density ratio on the secondary atomization under highly unstable condition, and the breakup processes under different density ratios are shown in Fig. 16. It was observed that the larger extent of the fragmentation occurs with increasing the density ratio. The droplet dynamics is notably influenced by the density ratio even if it exceeds 32, which is not consistent with the study of Alaburg et al. [195] who found that the deformation and breakup dynamics are independent of the density ratio when it exceeds 32 at small Oh number.

Other studies focus on the drag coefficient of deformable liquid droplets. Compared to the solid particle, the determination of drag coefficient of liquid droplet becomes more formidable due to surface pulsations, internal circulation, as well as deformation and breakup. Suh and Lee [196] firstly performed the calculation of drag and lift of a deformable droplet in shear flow by using the level set method. A feedback force that can maintain the droplet position is utilized to determine the acting force on the droplet. They found that the drag and lift forces depend strongly on the deformation characteristics. Yang et al. [194] investigated the drag coefficient of a droplet before breakup. It was shown that the drag coefficient is mainly determined by the recirculation region, i.e., a larger recirculation region leads to a higher drag coefficient.

Recently, Shao et al. [197] systematically studied the effects of Weber number, density ratio and viscosity ratio on the unsteady drag coefficient of a deformable droplet. The droplet Weber numbers were in the range of 1–10, and the density ratio and viscosity ratio were in the ranges of 6.25–40 and 2–1000, respectively. It was found that the unsteady term (including the density ratio) has the most significant effect on the unsteady drag coefficient and the Weber number secondly. The viscosity ratio has little effect on the drag coefficient owing to low Oh numbers in the study.

Although some progresses have been made for the single droplet deformation and breakup by using the level set method,

further investigations are required to explain the inconsistent results obtained by the simulations, such as the works by Yang et al. [194] and Aalburg et al. [195]. Furthermore, most of the above studies are in the range of low droplet Weber number. Droplet breakup in high Weber number regimes, the dominating breakup mechanism as well as the drop size distribution after breakup need to be explored. A general drag coefficient formulation of liquid droplet considering the effect of deformation and internal circulation also needs development.

4.2.2. Droplet collision

Droplet collision is expected to be a frequent event downstream of the fuel injector and could significantly modify the spray and combustion characteristics. Qian and Law [198] investigated binary droplet collision dynamics and summarized all the collision regimes in terms of the collision Weber number and the impact parameter. The behaviors of droplet collision were summarized as five distinct regimes, namely, coalescence after minor deformation, bouncing, coalescence after substantial deformation, coalescence followed by separation for near head-on collisions, and coalescence followed by separation for off-center collisions.

Tanguy and Berlemont [199] performed simulations of head-on and off-center droplet collisions by using the level set method in 2005. The collision Weber number is in the range of 23–60. The simulations could excellently reproduce the experimental observations from Ashgriz and Poo [200], as shown in Fig. 17. It is interesting to note that a very thin liquid layer was observed in the collision process during the simulation, which however is never to be captured by the experiment. This thin liquid layer is expected to be significant for the formation of satellite droplet.

Simulations by Pan and Suga [201] covered four regimes of collision: bouncing, coalescence, reflexive separation and stretching separation. The collision Weber number is in the range of 0.2–165. The numerical results indicated that the mechanism of bouncing collision is governed by the macroscopic dynamics. The mechanism of satellite droplet formation was associated with the end pinching and the capillary wave instability becomes dominant for larger impact parameter. Later, Balabel [202] performed simulations of two-dimensional binary droplet collision at relatively high collision

Weber numbers of 12.8, 156.8 and 460.8, corresponding to bouncing, coalescence and reflexive separation regimes, respectively. It was found that the surface tension is a stabilizing force in coalescence regime that prevents the separation of droplets, whereas it acts as a destabilizing force in reflexive separation regime that promotes the separation of droplets. However, it sometimes fails to simulate the droplet bouncing when the collision Weber number is very small. The simulation result indicates the coalescence regime, whereas the experimental result indicates the bouncing regime at the same collision Weber number. This is mainly attributed to the fact that two approaching droplets will artificially coalesce when their interfaces are sufficiently close to each other (typically at a distance on a grid cell) in the conventional level set method [201]. To overcome this problem, Kwakkel et al. [203] proposed an extension of the CLSVOF method with a coalescence/breakup model. In this method, each fluid droplet is described by a separated level set function, and the coalescence is identified based on a film drainage model that predicts if and when the two droplets will coalesce. Simulations were performed in the range of 2.3–61.4 for the collision Weber number. The excellent agreement with experimental data especially at the small collision Weber number demonstrates the capability of the method, but it should be noted that the collision dynamics is strongly dependent on the prescribed film drainage time. Balcazar et al. [204] proposed a multiple marker level set method to simulate the bouncing collision, in which the multiple markers are introduced to represent each droplet. The binary droplet collision with bouncing outcome also agrees well with the experimental data for the collision Weber numbers ranging from 2.27 to 9.33.

To summarize, numerical simulations of droplet collision nearly cover all the regimes and could reproduce the experimental observations with sufficient accuracy by using the level set method. However, some questions still remain. For example, the criterion for occurrence of each regime is not well defined, and numerical simulations with the level set method could help to distinguish each regime with sufficient resolution. Three-dimensional simulations of droplet collision with high collision Weber number is not sufficient, and collision dynamics of multiple droplets has not been established.

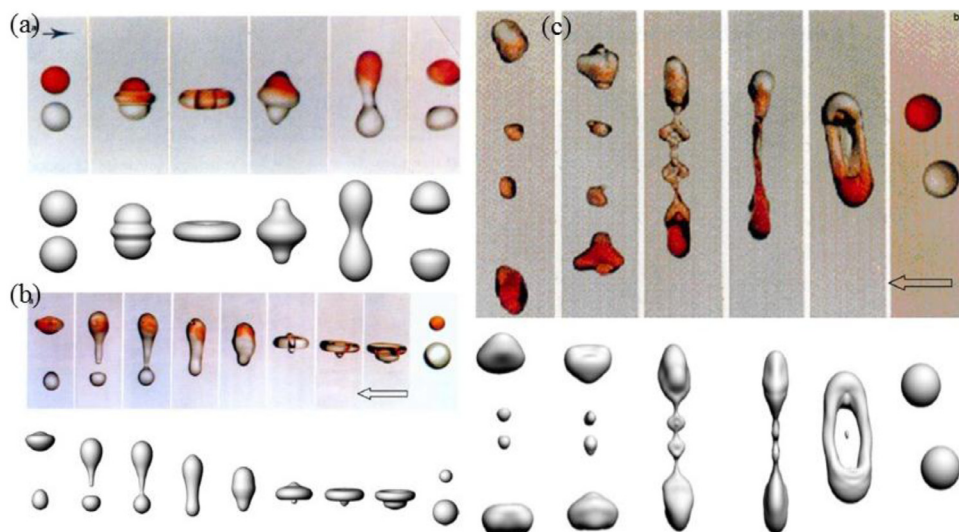


Fig. 17. The comparison between simulation and experiment (a) Head-on collision for two droplets with same sizes, $We_c = 23$, (b) Head-on collision for two droplets with different sizes, $We_c = 56$; (c) Off-center collision, $We_c = 23$ and $I=0.5$. The colorful pictures indicate the experimental results by Ashgriz and Poo [200]. Reprinted from Tanguy and Berlemont [199] with permission of Elsevier.

4.2.3. Droplet impact on surface

Drop impact on dry surface or liquid film is expected to be another type of drop collision. Based on the impact Weber number, Ohnesorge number and non-dimensional film thickness, droplet impact on surface can form various phenomena like drop receding, jetting, splashing and spreading [205].

Some studies focus on the validation of numerical methods by using the canonical set of droplet impact on surface. Yokoi [206] performed a simulation of droplet impact on a thin liquid layer by using the CLSVOF method. The impact Weber numbers were 426, 1706 and 6822, which remarkably influence the crown shape. The phenomenon was found to be sensitive to the grid resolution due to its multi-scale characteristics involving thin liquid layer and pinch-off droplets. To prevent numerical coalescence of droplet and liquid surface at small impact Weber number, a multiple marker CLSVOF method was developed by Coyajee and Boersma [207]. The idea of this method is similar to that of Kwakkel et al. [203] and Balcazar et al. [204] for simulating droplet collision. The drop trajectory and interfacial deformation observed from experiment can be well captured by this method. McCaslin and Desjardins [81] proposed a conservative level set method to simulate droplet impact on liquid film. The impact Weber number, Ohnesorge number and film thickness were 598, 0.0014 and 0.116, respectively, and $512 \times 1024 \times 1024$ grid points were used in the simulations. The radial growth of the splashing lamella was compared to theory and the numerical result of Rieber and Frohn [208], and good agreement has been achieved. The time evolution of growth of the splashing lamella is shown in Fig. 18, and it can be seen that the rim of the crown becomes unstable as the splashing lamella rises and ligaments form that finally pinch off into droplets. Drop splash onto a liquid film was also treated as a canonical set to validate a solver for DNS of gas-liquid flows with

the level set method by Shin et al. [209]. A highest resolution with 1024^3 meshes was run and detailed features of droplet ejection, crown formation and rim instability were observed.

Some other studies focus on the dynamics of droplet impact on surface. Lee et al. [210] investigated the two-dimensional splashing and spreading phenomena by using the level set method. Good agreement with experimental data was observed in the earlier stage of crown formation, but discrepancies appeared in the later stage of crown spreading. This indicated that the crown shape is axisymmetric in the earlier stage but shows three-dimensional characteristics later. Liang et al. [211] quantitatively discussed the influence of the impact Weber number, the Reynolds number, and the dimensionless film thickness on the crown diameter and height, and found that the crown height increases with the increasing of the impact Weber number. The pressure difference in the neck region and the velocity discontinuity have significant effect on the jet formation. The increase in the impact Weber number and drop diameter contributes to the formation of bubble rings below the impacting droplet. Guo et al. [212] investigated the effects of impact velocity and the film thickness on the crown diameter. It was shown that the higher the impact velocity is, the earlier the splash emerges, and the spreading diameter decreases with the increasing of the film thickness. Chai et al. [213] investigated the incipient droplet impact by using a conservative level set method. The impact Weber number, Ohnesorge number and film thickness were 297, 0.0019 and 0.29, respectively. It was found that the pressure gradient and vortex are responsible for the neck jet formation and evolution. With the inclined angle of the surface increasing, the vortex effect becomes larger in the back side while the pressure gradient is still dominant in the front side. It was also observed that air bubbles are trapped below the impacting droplet even though there is no explanation.

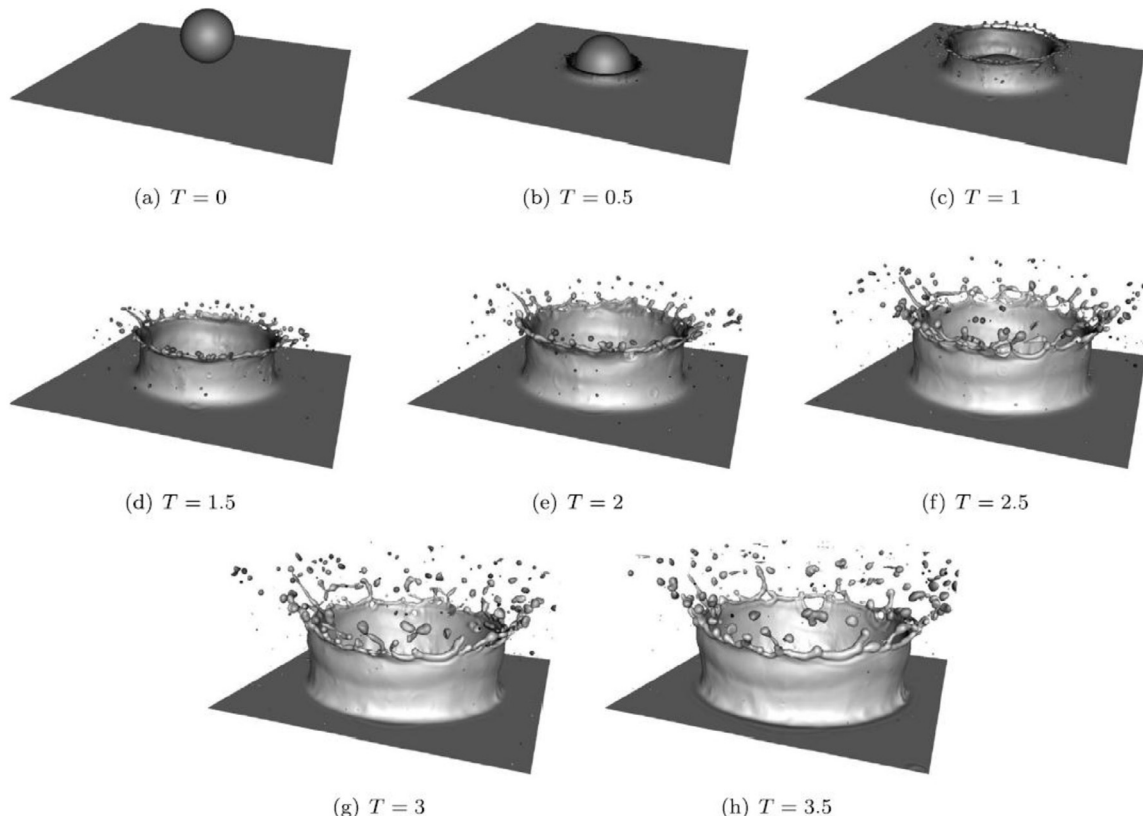


Fig. 18. Growth of the splashing lamella resulting from drop impact on liquid film. Reprinted from McCaslin and Desjardins [81] with permission of Elsevier.

Droplet impact on different types of surfaces has also been investigated recently. Liu et al. [214] investigated the dynamic characteristics of a droplet impacting a hydrophobic tube. It was found that the surface hydrophobicity has a great influence on the dynamic characteristics of the film spread. The pressure difference between the inside and outside of the liquid film and the location of the low pressure dominate the film spread, rebound and splash. Yan and Li [215] performed simulation of droplet impact on micro-scale rectangular grooved surface. The effects of groove width, contact angle and impact velocity on the dynamic of the droplet impact at low Weber numbers were investigated. It was found that the vertical spreading diameter is less than the parallel spreading diameter, and the dynamic characteristic of droplet impact is influenced by both the contact angle and the groove width.

The above studies demonstrate that droplet impact on surface succeeds to act as a canonical benchmark for validation of numerical method on one hand. On the other hand, the mechanisms of droplet impact on surface have been explored including bubble entrainment below the droplet, the neck jet formation, and crown formation that are important in the impact dynamics. However, the explanation on the bubble entrainment is not sufficient with the present low resolution of the impact region, and the dominant mechanism of producing secondary droplets by splashing has not yet been investigated [216]. In addition, multi-drop impact that is usually encountered in applications has received far less attention. All these issues need further investigations.

4.2.4. Atomization with turbulence

In realistic spray combustion applications, the atomization process usually occurs with turbulence. For droplets that are smaller than the smallest turbulent length scale (the Kolmogorov scale, η), point-particle assumption is usually used. For liquid structures/droplets that are larger than η in dense spray region, studies are limited but have drawn much attention with the recent development of the level set method [217].

Li and Jaberi [218] performed a simulation of two-dimensional homogeneous flow with liquid plane sheet to investigate the turbulence-interface interaction by using the particle level set method. The density ratio and viscosity ratio are both in the range of 1–20. It was found that the rate of change of the interface area is related to the work done by the surface tension. The surface tension increases the turbulent kinetic energy when the interface experiences compression, while it damps the turbulent kinetic energy when the interface experiences stretching. Furthermore, the surface tension was found to generate strong vortical motions close to the interface by the baroclinic torque effects. Trontin et al. [219] performed a three-dimensional simulation of a freely decaying homogeneous isotropic turbulence (HIT) flow with a liquid plane sheet to understand interactions between small turbulent scales and interface. The densities and viscosities are the same for both phases. Two types of turbulence/interface interactions have been obtained. For large Weber number, the energy is transferred from the turbulence to the interface for the coalescence of small droplet into larger drops. However, for lower Weber number, the interfacial energy is given back to the fluid. For all studied Weber numbers, anisotropy and vorticity appear near the interface resulting from the turbulence/interface interaction.

Recently, Shao et al. [220] have performed simulation of droplet breakup in a forced HIT flow to investigate the interaction between vortical structures and the interface by using a mass-conserving level set method. The densities and viscosities are the same for both phases. The temporal evolution of the liquid/gas interfaces is shown in Fig. 19. It was observed that the interface is slightly wrinkled at the early time and stretched and rolled up to numerous tube-like/blob-like structures at the later times. The vorticity tends to be perpendicular to the normal of the large-scale interface at an

early stage, and subsequently the normal alignment is mitigated for large Weber numbers. This indicated that small droplets with strong surface tension can resist the deformation induced by local turbulent straining motion in the statistically stationary state.

The DNS database of atomization with turbulence has also been used to improve atomization model. Duret et al. [221] performed simulations of eight droplets breakup in a HIT flow over a large range of liquid volume fractions and the database have been utilized to improve the ELSA model [222]. It was found that the liquid kinetic energy or the Favre averaged kinetic energy in the improved equilibrium Weber number is close to the kinetic energy on the interface. A statistical analysis of the equilibrium Weber number was then carried out to verify and improve the definition given by the ELSA model. Ensemble averaging of the time evolution of the interface density was also conducted to verify the interface density equation. The improved ELSA model was compared with the DNS and good agreement was achieved. Herrmann [10] proposed a dual-scale modeling approach for phase interface dynamics in the LES context based on the DNS data in a HIT flow. A resolved realization of the phase interface dynamics was explicitly filtered to close the unclosed terms related to the phase interface, including the effects of sub-filter turbulent eddies, surface tension, and dissipation. Satisfactory agreement between LES and DNS was obtained.

The progress in interface-resolved simulation of atomization with turbulence is associated with the development of the level set method and the advances in supercomputer. The liquid breakup in HIT flow has been widely used to investigate turbulence/interface interaction and improve atomization model. However, due to the complexity, experimental data are required to validate the DNS results [217]. In addition, all the present DNS studies with fully resolved interface limit the density ratio to the range of 1–30, which is expected to be higher in realistic spray combustion.

4.3. Integrated simulation of atomization

As aforementioned, atomization is a typical multi-scale phenomenon, in which the size of the smallest droplet may be several orders smaller than the size of the atomizing liquid jet. This multi-scale nature introduces a fundamental challenge to the interface-resolved simulations of atomization. Specifically, at least four to eight grid points across the droplet diameter are required to obtain a physically reasonable representation of the droplet [152,223]. As a result, huge computational resources would be consumed for such integrated simulations of atomization.

To reduce the computational cost, multi-scale coupling methods have been developed, in which the Eulerian method is used to capture the large-scale interfaces and the Lagrangian point-particle (LPP) method is used to track the small-scale droplets, as illustrated in Fig. 20. The coupling procedure usually consists of identification of liquid structure, removal from the Eulerian description, transfer to the Lagrangian description and, if necessary, reverse transfer to the Eulerian description. Crucial to such coupling methods is the conversion criterion between the two description frameworks.

Kim et al. [146,147] used the level set method with a sub-grid Lagrangian breakup model to simulate the breakup of a liquid round jet. Two conversion criteria for drop transfer [146] were proposed as $V_D \leq 2V_{cv}$, $r_{max} < 2r_{sphere}$, where V_D is the drop volume, V_{cv} is the grid cell volume, r_{max} is the maximum distance between the center of mass and the surface of the drop, r_{sphere} is the radius of a corresponding sphere such that $4/3\pi r_{sphere}^3 = V_D$. Furthermore, a capillary breakup model [147] was inserted as Lagrangian drops when pinching-off of ligaments is not resolved on the level set grid. This method is claimed to be able to conserve the mass as well as reduce the computational cost. Herrmann [150] proposed

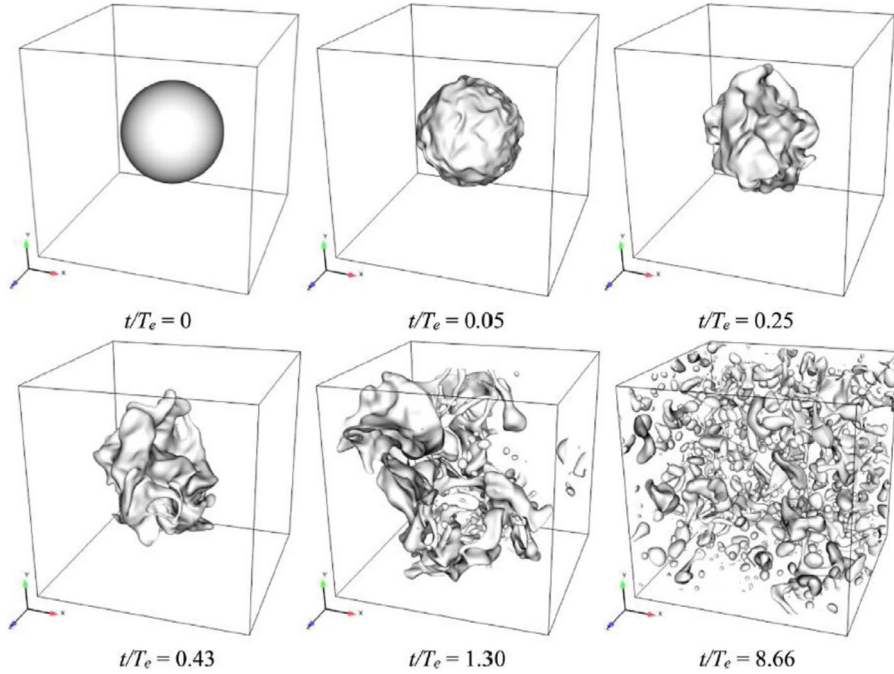


Fig. 19. The temporal evolution of the liquid/gas interface, where T_e is the eddy turnover period. Reprinted from Shao et al. [220] with permission of Elsevier.

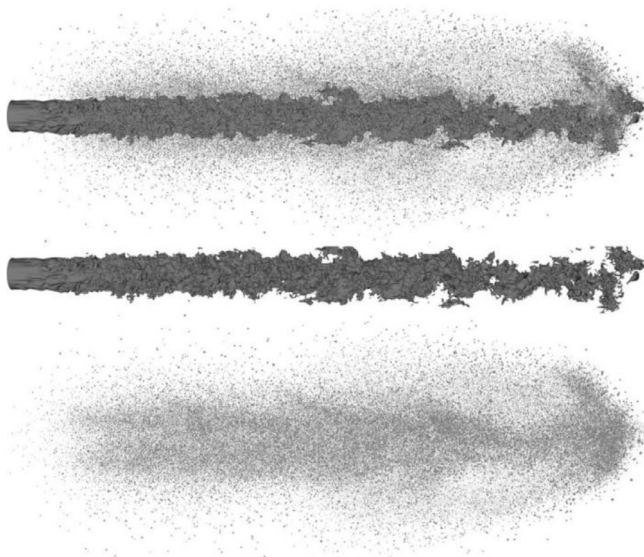


Fig. 20. Atomization of turbulent liquid jet. The liquid core and spray (top) are described by the Eulerian captured phase interface (middle) and the Lagrangian tracked particles (bottom). Reprinted from Herrmann [150] with permission of Elsevier.

a parallel Eulerian-Lagrangian coupling procedure to simulate the straight jet. A recursive algorithm was used to identify the liquid structures. Then a threshold volume as well as an eccentricity measure threshold was used as the conversion criteria, based on which the transfer from the Eulerian to the Lagrangian description was formulated. The reverse transfer was given by simply re-evaluating the local level set field due to drop/drop collision or drop collision with the Eulerian structures. Arienti et al. [179] used a Lagrangian model for postbreakup tracking of droplets with block-structure AMR and the CLSVOF method for the impinging jet simulation. Similarly, a threshold volume and the drop

sphericity were used as the conversion criteria. The coupling procedure mainly consists of three steps as droplet identification, conversion criteria from Eulerian to Lagrangian representation, and Lagrangian droplet generation and transport. The drop size distribution was in good agreement with the experimental data although the reverse transfer from Lagrangian to Eulerian description was not considered. This coupling method has been further applied to simulations of swirling jet [182] and crossflow jet [177].

Tomar et al. [163] performed a multi-scale simulation of primary atomization by using the interface capturing method coupled with a two-way coupling Lagrangian particle tracking model. A threshold volume was used for the Eulerian-Lagrangian transformation, and the Lagrangian particles were reversely transformed to Eulerian description when the particles are less than a grid cell. The collisions between droplets were predicted by using a spatial-hashing algorithm. Ling et al. [223] put a focus on the conversion and momentum coupling between the Eulerian and Lagrangian representation. The conversion criteria between Eulerian and Lagrangian representation depend on the droplet volume, aspect ratio, and position. The feature of the momentum coupling lies in distributing the coupling force back to the resolved flow over a length scale of 5–10 times of the droplet diameter. This approach proves to faithfully recover the large-scale features of gas-assisted atomization.

Zozio et al. [224] developed an improved multi-scale Eulerian-Lagrangian method for simulation of atomization. The sphericity criterion was used only for the conversion from Eulerian to Lagrangian representation. The Lagrangian droplets were represented by two inclusions, i.e., small inclusion that the droplet size is lesser than the local grid size for drag-force model, and medium inclusion that the droplet size is greater than the local grid size for intermediate treatment. The procedure includes detection of droplets, transformation criteria, tracking, and drop-interface collision. Numerical tests showed a good performance in particular for the meso-scales in which liquid structures can be captured on a few grid cells. It should be noted that the medium droplets that hold 1–4 grid cells can not be sufficiently resolved, and also fail

the Lagrangian point assumption. For such dilemma, the treatment proposed by Ling et al. [223] and Zozio et al. [224] to conserve the momentum is a better choice.

Significant efforts have been made to develop coupled Eulerian and Lagrangian methods for integrated simulations of atomization. The focus has moved from one-way coupling in early studies to two-way coupling in recent studies. Numerical results seem to faithfully recover the overall characteristics of atomization. However, the details of the conversion and the consistency of position, mass, and momentum need further investigation. The conversion criteria have several types that should be unified. The post-transfer velocity field will be changed and the drop dynamics or the drag induced gaseous flow has been simplified. These issues require further attention.

4.4. Interface with evaporation

Interfaces with evaporation are always encountered in dense spray zone and deformable droplets, but it is difficult to model the evaporation process with these irregular interfaces. With the level set method, it is feasible to directly simulate interfaces with evaporation, as introduced in Section 3. Here we only focus on the phenomena of liquid structures with evaporation or droplet impact on hot surfaces. Under the latter condition, a thin vapour layer may generate between the droplet and the surface, causing the so-called Leidenfrost effect [225].

Early studies on the interface-resolved droplet with evaporation are dependent on empirical models. With the help of vapor flow model and heat transfer model, Ge and Fan performed simulations of liquid droplet impact on a flat surface [226,227] and droplet-particle collision [228,229] in the Leidenfrost regime by using the level set method. In these studies, the droplet dynamics and droplet-vapor-surface/particle heat transfer have been analyzed with different impact Weber numbers. Some interesting results have been obtained, for example, the subcooled impact yields a thinner vapor layer and a higher heat transfer rate compared to the saturated impacts.

Later, without empirical models, Gibou et al. [133] proposed a level set method for multiphase flow with phase change. The evaporative mass transfer was calculated at per unit droplet surface area. The temperature on the interface was assumed to be saturated and the energy equation was solved in both phases. The mass transfer and heat transfer were calculated by considering the jump conditions across the interface. Two-dimensional evaporation of a drop was simulated to validate the method. Chatzikyriakou et al. [230] also performed a simulation of droplet-hot wall interaction without empirical models. Evaporative mass transfer was approximated by specifying a uniform mass transfer rate and the energy equation was not solved. The droplet rebounding phenomenon was simulated in two dimensions and good agreement with experimental observation was observed.

By using the level set method, Son and coworkers conducted simulations of microdroplet evaporation on a heated surface [143], the Marangoni effect [231], the particle motion [232] and the particle-laden droplet evaporation with the Marangoni effect [233]. A dynamic contact angle model was incorporated into the method to consider the change at the liquid-gas-solid interline. Both the temperature and mass fractions were considered in the method. It was found that the droplet life depends strongly on the wall temperature. The Marangoni effect increases the liquid velocity inside the droplet and the gas velocity along the surface. The particle accumulation near the contact line is consistent with the experimental observation. Tanguy et al. [119] proposed a level set method for evaporating two-phase flows. A local evaporation mass flow rate per unit of surface area was defined and the GFM was used to handle jump conditions for heat and mass transfers. A projection

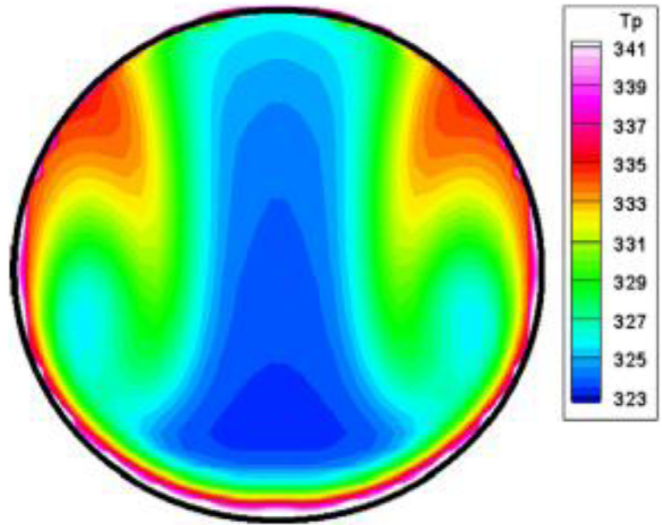


Fig. 21. Temperature field inside the falling drop at $t=0.0075\text{ s}$ from [119]. Reprinted from Tanguy et al. [119] with permission of Elsevier.

method was set up to impose a divergence-free condition. The d^2 law was reproduced through simulation of a static drop evaporation. Simulation of a water droplet moving in air was also performed and the temperature inside the droplet is shown in Fig. 21. It was observed that a vortex due to the viscosity jump between the liquid and gas phases can lead to non-uniform spatial temperature distribution inside the drop. This also implies that the importance of defining the local evaporation rate per unit of the surface area.

The droplet is usually considered to be at saturated condition in early studies. However, the distinction between evaporation and boiling is not always possible in some specific situations involving heterogeneous thermodynamic conditions on the interface. Thus, the interface temperature can locally reach the boiling temperature but be cooler in other areas. To overcome this issue, Villegas et al. [144] proposed a novel numerical method that allows dealing with both evaporation and boiling on the interface. The feature of this method lies in imposing Robin boundary condition. Simulation of an impacting droplet on a hot plate including Leidenfrost effect was performed and the temperature field in the liquid phase at different times is presented in Fig. 22. The transition between the evaporation regime and boiling regime was clearly visualized, and the formation of a thin saturation vapor layer was observed between the hot wall and the interface during the droplet spreading. Villegas et al. [137] further investigated the droplet impact on a hot surface for different impacting Weber numbers ranging from 7 to 45. It was found that the droplet heating increases with the impacting Weber numbers, and the simulation allows for accurate description of the multi-scale characteristics involving fluid dynamics and coupled heat and mass transfer.

Duret et al. [221] used a passive scalar to represent the evaporation and mixing process in a two-phase HIT flow with the level set method to capture the gas-liquid interface. The method was restricted to low evaporation rate in which the interface was barely affected by the evaporation process. The statistical analysis of the vapor field was performed and it showed that the beta PDF, frequently used in combustion modeling, is not adequate to represent the scalar mixing when interface is involved. In addition, the results showed that the evaporation process does not affect the spectrum shape of the scalar but change the energy level of the scalar.

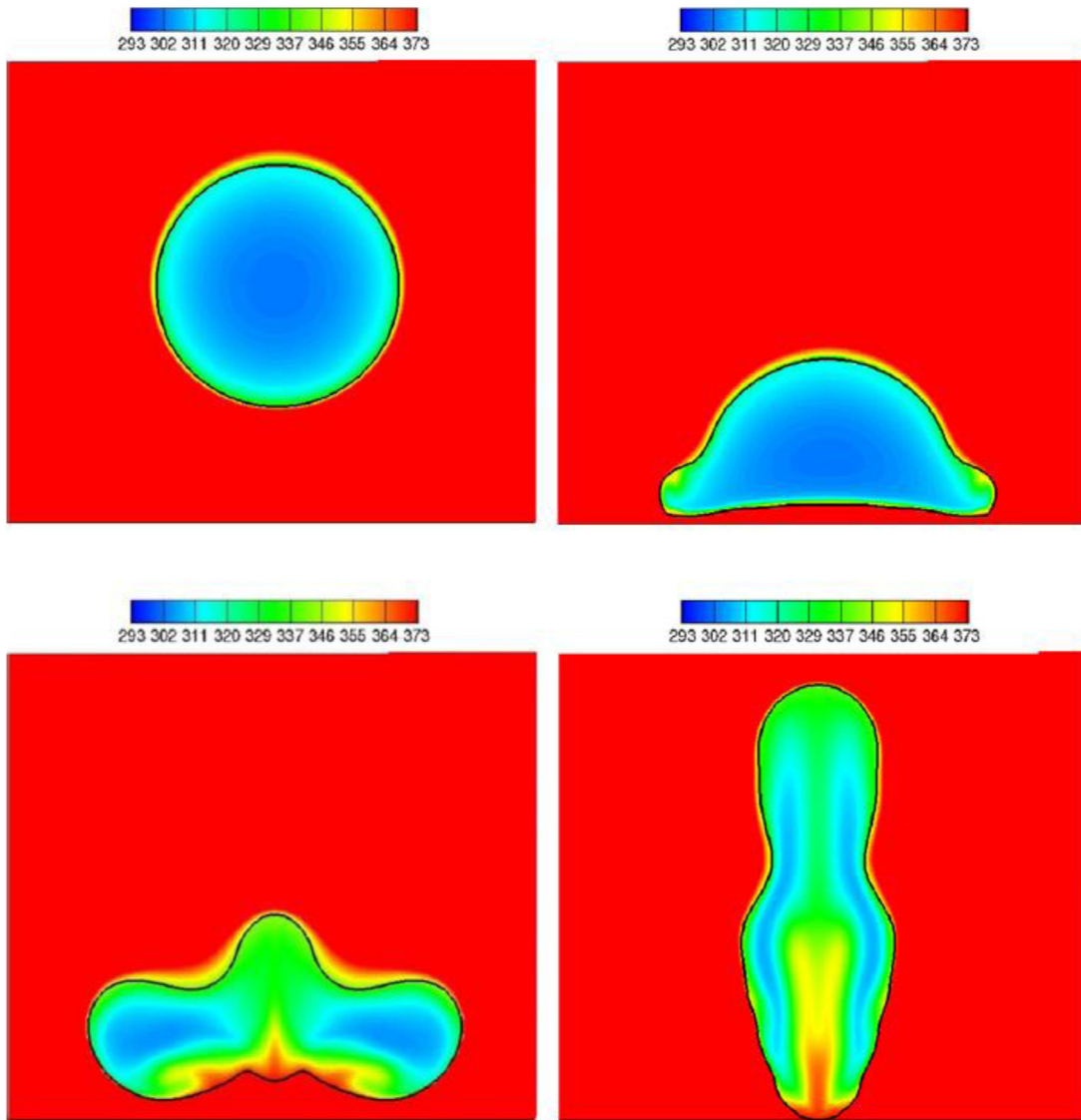


Fig. 22. Temperature field in the liquid phase and interface evolution (in black) during the impingement of a levitating droplet on a hot wall at different time ($t_1 = 9.83 \times 10^{-5}$ s, $t_2 = 1.36 \times 10^{-4}$ s, $t_3 = 1.57 \times 10^{-4}$ s, $t_4 = 2.69 \times 10^{-4}$ s). Reprinted from Villegas et al. [144] with permission of Elsevier.

Recently, Fechter et al. [234] proposed an approximate Riemann solver for compressible flow with phase transition and surface tension with the level set method for capturing the interface. Simulation of a shock-droplet interaction was performed and it was demonstrated that the method can provide a fast and accurate resolution of phase transfer effect with much lower costs.

Li et al. [178] performed simulation of liquid fuel atomization and evaporation in crossflow with an advanced method. The CLSVOF method with AMR technique was used to capture the interface, and the Lagrangian single-particle model was applied to describe the small-scale droplets. Two-way transition and coupling between gaseous phase and Lagrangian droplets were considered. The liquid jet Weber number and Reynolds number were 180 and 3490, respectively. It was found that when the injected liquid is colder than the crossflow gas, the vapor downstream distribution is center peaked which is related to the relative sizes and evaporation time of the droplets.

In addition, interface-resolved simulations of relative gas-liquid with the level set method for capturing the interface have been developed in the recent years. Shao et al. [142] developed a com-

putational framework for interface-resolved simulation of simultaneous atomization, evaporation and combustion, in which interface is described by using the level set method, discontinuity across the interface is treated by using the GFM, and one-step global reaction chemistry of *n*-heptane is used for the vapor combustion. This method can treat both conditions that the gas temperature is lower or higher than the saturation temperature, and the performance has been validated by several benchmark simulations. Integrated simulation of droplet collision and combustion was also carried out to evaluate the accuracy and robustness of the method. Zoby et al. [235] performed simulations of regularly ordered kerosene droplet arrays in inert and reactive convective environments by using a mass conservative level set method. Evaporation rates were compared to two evaporation models based on heat and mass transfer numbers. It was found that two empirical evaporation models are of limited success to predict the evaporation rates of dense sprays, and there is no evident correlation between the evaporation rates and the subgrid kinetic energy. Haruki et al. [236] investigated transient flame propagation in *n*-decane droplet arrays by using the level set method. Three different modes of flame propagation

were successfully reproduced as observed in experiment. The flame propagation speed was accurately predicted, on which the radiative heat transfer had an essential influence. Shinjo and coworkers investigated droplet/turbulence interaction during primary atomization [237,238] and fuel droplet puffing and microexplosion [239,240]. It showed that mixing by turbulent eddies around the droplets is enhanced more strongly than molecular diffusion, and group combustion is likely to occur. The droplet-generated mixing enhancement effect should be included in the classical point-source model. For microexplosion/puffing of a water-in-oil emulsion droplet, it was found that the temperature field is distorted by the velocity field, but the Hill's vortex is not formed because of the weak distortion. A model was then proposed to reproduce the temperature field inside the droplet which is a key initial condition of microexplosion/puffing.

Significant progresses have been obtained for simulations of interface with evaporation by using the level set method in the last decade. The empirical vapor layer model and heat transfer model used in early studies were replaced by accurate and direct methods of considering the jump conditions across the interfaces. With these more accurate methods, the dynamics and heat/mass transfer inside or around the interfaces could be reproduced, and new phenomena were observed. However, systematical investigation of the droplet-turbulence-evaporation-combustion interaction mechanisms is still limited, especially in realistic spray combustion conditions.

5. Summary and outlook

The level set method has achieved a significant success in multiphase simulations over the past twenty years. In this article, methodology development of the level set method and applications to detailed numerical simulation of atomization/evaporation have been reviewed. For methodology development, the state-of-the-art attempts to improve the mass conservation property of the level set method can be classified into two categories, namely, improvement of the discretization of the level set equation and improvement of the re-initialization process. The interface refined level set method coupling with the VOF method is believed to be the most attracting tool for simulations of large-scale atomization process. New challenges are highlighted when simulating atomization with evaporation by using the level set method. The treatment of three important issues has been discussed including jump conditions across the interface, insurance of divergence-free velocity field, and unified calculation of evaporation rate. Recently, the efforts of coupling of numerical method for atomization and evaporation even reaction have been increasing and it is expected to be the most accurate way to directly simulate the overall spray combustion process. These improvements in methodology provide a faithful tool to simulate atomization and evaporation.

With regard to the applications of the level set method to simulations of atomization and evaporation, the focus is placed on the primary atomization, secondary atomization, and evaporation on irregular interface. The overall large-scale structures observed in experiments can be successfully reproduced by using the level set method. For instance, the subtle phenomena, such as the sheet formation, ligaments or hole formation from the sheet, and the impact region of droplet impact on a liquid film, can be captured that are difficult to be observed in experiments. With the help of these observations, the corresponding mechanisms related to atomization and evaporation have been partially identified.

Despite of significant progresses, several challenges and unsolved issues still exist in detailed numerical simulation of atomization and evaporation with the level set method. The first is related to the fidelity of the smaller droplet in large-scale simulations of atomization. On one hand, the droplets especially those

smaller than the Kolmogorov scale are not fully resolved in most current simulations of atomization. One should admit it that resolving the smallest droplet in realistic atomization is unfeasible for the present interface capturing or tracking methods owing to huge computational cost. Hence the primary work we can do is to assess the influence of the smaller droplets on the overall large-scale structures. On the other hand, the current numerical results of drop size distribution are mostly not grid convergence, which can provide incorrect information for spray combustion simulation. The integrated Eulerian-Lagrangian method may be an effective alternative to represent the overall atomization/evaporation process.

Secondly, there is a lack of general understanding of the physical mechanisms of atomization process especially in realistic spray combustion conditions. Although various physical mechanisms at different regimes have been proposed by different researchers based on detailed numerical simulations of atomization, some of them are contrary to each other, even under the same conditions. The consistency with the development of interfacial instability and the reason that triggers the atomization by interfacial instability have not yet been achieved.

Thirdly, more attention should be paid to the improvement of sub-grid model, atomization model, and droplet/evaporation model that are used in the RANS/LES context. On one hand, in classical CFD simulations of spray combustion, the accuracy of atomization model is very important especially for realistic applications, but the state-of-the-art atomization models rely heavily on theoretical assumptions or empiricism. To this end, the database of atomization via interface-resolved DNS can be used to improve the atomization model and the subgrid model that are used in the RANS/LES context. On the other hand, for combustion applications, the classical drag coefficient correlation, single droplet dynamic, single droplet evaporation model, liquid film evaporation model, turbulent mixing model and sub-grid models are usually used. It is expected that these models are different with and without combustion. There is a need to validate and improve these models based on the DNS database of atomization with evaporation and combustion. Unfortunately, limited improvement has been made along this line in the literature.

Finally, there is a great lack of investigation on spray relevant issues by using the level set method, such as, the nozzle internal flow effect on the atomization process, the electrohydrodynamic (EHD) atomization, and the coupling with magnetic field. It will be interesting to investigate those effects in the future.

Acknowledgments

This work is financially supported by the National Natural Science Foundation of China (Nos. 91741203 and 91541202), China Postdoctoral Science Foundation (2018M642428) and Zhejiang University Education Foundation Global Partnership Fund.

Supplementary material

Supplementary material associated with this article can be found, in the online version, at doi:[10.1016/j.pecs.2019.03.001](https://doi.org/10.1016/j.pecs.2019.03.001).

Appendix A

This appendix presents the mathematical formulations of the PDE extrapolation and the FMM extrapolation.

Taking the linear extrapolation as an example, the PDE extrapolation extends A in the normal direction by solving the following sequent equations to steady state [134]:

$$\frac{\partial A_n}{\partial t} = -H(\phi) \vec{n} \cdot \nabla A_n \quad (47)$$

$$\frac{\partial A}{\partial t} = -H(\phi)(\vec{n} \cdot \nabla A - A_n) \quad (48)$$

where $A_n = \vec{n} \cdot \nabla A$ corresponds to the directional derivative in the normal direction, \vec{n} is the unit normal vector pointing to the unknown subdomain and is a unit Heaviside function. Note that the Heaviside function is used simply to not disturb the values in known subdomain. In particular, $H=0$ in the known subdomain and $H=1$ in the unknown one. A second-order upwind scheme is employed to discretize the above PDEs. Once Eq. (47) reaches the steady state, Eq. (48) reduces to $\vec{n} \cdot \nabla A_n = 0$, indicating that A_n is a constant in the normal direction. The obtained A_n -field appears as a source term in Eq. (48). Once Eq. (48) reaches the steady state, the normal derivative of the finally obtained A equals to A_n .

Instead of converging the above PDEs to steady state, the FMM extrapolation [135] solves the non-homogeneous Hamilton–Jacobi equations, which are mathematically identical to the steady-state PDEs, using the FMM. For instance, the corresponding Hamilton–Jacobi equation of Eq. (48) reads

$$\nabla A \cdot \nabla \phi = A_n \quad (49)$$

after recalling Eq. (2). Upwind finite difference stencils are used to discretize Eq. (49) by solving

$$\begin{aligned} S_x^-(D_x^- \phi_{i,j,k} \cdot D_x^- A_{i,j,k}) + S_x^+(D_x^+ \phi_{i,j,k} \cdot D_x^+ A_{i,j,k}) \\ S_y^-(D_y^- \phi_{i,j,k} \cdot D_y^- A_{i,j,k}) + S_y^+(D_y^+ \phi_{i,j,k} \cdot D_y^+ A_{i,j,k}) \\ S_z^-(D_z^- \phi_{i,j,k} \cdot D_z^- A_{i,j,k}) + S_z^+(D_z^+ \phi_{i,j,k} \cdot D_z^+ A_{i,j,k}) = A_{n,i,j,k} \end{aligned} \quad (50)$$

where $D_{x,y,z}^\pm$ are first order upwind finite difference notations, and the switches S_x^\pm are defined as

$$\begin{aligned} S_x^+ &= \begin{cases} 1 & \text{if } \max(D_x^- \phi_{i,j,k}, -D_x^+ \phi_{i,j,k}, 0) = -D_x^+ \phi_{i,j,k} \\ 0 & \text{otherwise} \end{cases} \\ S_x^- &= \begin{cases} 1 & \text{if } \max(D_x^- \phi_{i,j,k}, -D_x^+ \phi_{i,j,k}, 0) = D_x^- \phi_{i,j,k} \\ 0 & \text{otherwise} \end{cases} \end{aligned} \quad (51)$$

McCaslin et al. [135] found that if second order convergence accuracy in a narrow band is sufficient for a given application, then the FMM extrapolation should always be used, as it provides the same accuracy as the PDE at a significantly reduced cost. If higher rates of convergence is required, a high-order polynomial PDE method is preferable.

Appendix B

The standard projection method for the incompressible Navier–Stokes equations consists of the three steps. In particular, an intermediate velocity field at a new time step $n+1$ is firstly calculated by advancing the momentum equation without pressure term,

$$\frac{\vec{u}^{*} - \vec{u}^n}{\Delta t} = -\vec{u}^n \cdot \nabla \vec{u}^n + \frac{1}{\rho^n} \nabla \cdot \left(\mu \left[\nabla \vec{u}^n + (\nabla \vec{u}^n)^t \right] \right) + \vec{g} \quad (52)$$

Then the divergence-free condition gives the pressure Poisson equation,

$$\nabla \cdot \left(\frac{\nabla p^{n+1}}{\rho^{n+1}} \right) = \frac{\nabla \cdot \vec{u}^*}{\Delta t} \quad (53)$$

And finally the velocity field is corrected to ensure continuity using the pressure gradient,

$$\vec{u}_l^{n+1} = \vec{u}_l^* - \Delta t \frac{\nabla p^{n+1}}{\rho^{n+1}} \quad (54)$$

For evaporating two-phase flows, the projection method is solved separately in each phase and the GFM is used to treat the discontinuities of pressure and velocity.

In [119], to preserve the divergence-free condition on the interface, a complex improvement of the liquid velocity field extension has been developed by Tanguy et al. It consists in solving an additional Poisson equation for liquid velocity field in the gaseous domain:

$$\nabla \cdot \left(\frac{\nabla p^{ghost}}{\rho^{n+1}} \right) = \frac{\nabla \cdot \vec{u}_l^*}{\Delta t} \quad (55)$$

The obtained ghost pressure enables the definition of the extension of the liquid velocity field

$$\begin{cases} \vec{u}_l^{n+1} = \vec{u}^* & \text{if } \phi > 0 \\ \vec{u}_l^{ghost} = \vec{u}_l^* - \Delta t \frac{\nabla p^{ghost}}{\rho^{n+1}} & \text{if } \phi < 0 \end{cases} \quad (56)$$

whereas the ghost values of the gas velocity are simply defined by Eq. (39).

Appendix C

To complete the HFM of evaporation, one needs to predetermine the interface temperature T^Γ , which can be customarily set to the equilibrium saturation temperature corresponding to the interface pressure p^Γ . If the thermodynamic equilibrium on the interface is applied, then T^Γ is uniquely determined through the Clapeyron relation

$$T^\Gamma = T_{sat}(p^\Gamma) \quad (57)$$

Eq. (57) is adequate and convenient for macroscale boiling problems involving plane interface. For a more general application this review concerns, however, the pressure will jump across the interface due to capillary, viscous and phase change effects as Eq. (36) addresses. In particular, the equilibrium saturation temperatures corresponding to the interface pressure in the gas and liquid phases are not consistent:

$$T_{sat}(p_l^\Gamma) \neq T_{sat}(p_g^\Gamma) \quad (58)$$

That is to say, the local thermodynamic equilibrium implies that the interface temperature is continuous on the interface only if the pressure is continuous, and jumps if the pressure jumps. Note that, the temperature discontinuity cannot be eliminated by rigorous application of first principles [241]. In Shankar and Deshpande [242], the temperature distribution in mercury–vapor phase change between plane liquid surfaces shows jumps across the interface as large as almost 50% of the applied temperature difference.

The temperature discontinuity lead to a question of what value should be chosen for T^Γ . Two choices of thermal boundary conditions are possible in the literature such as Huang and Joseph [243]. The first one assumes temperature should be continuous on the interface

$$T^\Gamma = T_l^\Gamma = T_g^\Gamma = T_{sat}(p_\infty) \quad (59)$$

where p_∞ is the reference ambient system pressure. Although Eq. (59) physically violates the thermodynamic equilibrium because $T_{sat}(p_l^\Gamma) \neq T_l^\Gamma = T_g^\Gamma \neq T_{sat}(p_g^\Gamma)$, it allows thermal equilibrium of the two phases. The second one, using the kinetic theory, assumes local thermodynamic equilibrium for both phases, and allows a temperature discontinuity on the interface

$$T_{sat}(p_l^\Gamma) = T_l^\Gamma \neq T_g^\Gamma = T_{sat}(p_g^\Gamma) \quad (60)$$

The correct choice of the interface temperature boundary condition is still an unresolved issue. But according to Juric and Tryggvason [244], both approaches lead to the same concept: an interfacial resistance to mass transfer across the interface. Correspondingly, they proposed a general procedure to address the thermal interface condition. They began with the principle of balance of entropy

across the interface, and integrated the equation from (T_{sat}, p_∞) to (p^Γ, T^Γ) to give an expression for the interface temperature

$$\begin{aligned} T^\Gamma - T_{sat} = & - \frac{T_{sat}}{h_{lg}} \left[\frac{1}{\rho} \right]_\Gamma (p^\Gamma - p_\infty) + \frac{1}{h_{lg}} [C_p]_\Gamma (T^\Gamma - T_{sat})^2 \\ & + \frac{\sigma \kappa T_{sat}}{2h_{lg}} \left(\frac{1}{\rho_l} + \frac{1}{\rho_g} \right) \\ & + \frac{T_{sat}}{2h_{lg}} \left[\frac{1}{\rho} \right]_\Gamma [((\vec{\tau}_l + \vec{\tau}_g) \cdot \vec{n}) \cdot \vec{n}] - \frac{\dot{\omega}}{\gamma} \end{aligned} \quad (61)$$

where $\vec{\tau} = \mu(\nabla \vec{u} + \nabla \vec{u}^t)$ is the deviatoric stress tensor, and γ is the kinetic mobility, describing the resistance to mass transfer across the interface. The interface pressure can be defined as the average of the interface pressures in the liquid and gas phases. In [244], they also performed a scale analysis to assess the contribution of different effects, i.e. the right hand terms of Eq. (61). In respect to problems this review concerns, the interface temperature deviation is usually weak, and the contribution of these different effects is negligible. When all of the right hand terms are discarded, Eq. (61) reduces to the first approach of Eq. (59). Indeed, this simplification proves to be effective in many situations [117,144].

References

- [1] Kim J. Spray cooling heat transfer: the state of the art. *Int J Heat Fluid Flow* 2007;28(4):753–67.
- [2] Zhou ZF, Chen B, Wang YS, Guo LJ, Wang GX. An experimental study on pulsed spray cooling with refrigerant R-404a in laser surgery. *Appl Therm Eng* 2012;39:29–36.
- [3] Luo K, Pitsch H, Pai MG, Desjardins O. Direct numerical simulations and analysis of three-dimensional n-heptane spray flames in a model swirl combustor. *Proc Combust Inst* 2011;33:2143–52.
- [4] Irandejad A, Banaeizadeh A, Jaberi F. Large eddy simulation of turbulent spray combustion. *Combust Flame* 2015;162:431–50.
- [5] Ashgriz N. *Handbook of atomization and sprays: theory and applications*; 2011.
- [6] Xiao F, Dianat M, McGuirk JJ. Large eddy simulation of single droplet and liquid jet primary breakup using a coupled level set/volume of fluid method. *Atomization Spray* 2014;24:281–302.
- [7] Xiao F, Dianat M, McGuirk JJ. LES of turbulent liquid jet primary breakup in turbulent coaxial air flow. *Int J Multiphas Flow* 2014;60:103–18.
- [8] Xiao F, Dianat M, McGuirk JJ. Large eddy simulation of liquid-jet primary breakup in air crossflow. *AIAA J* 2013;51:2878–93.
- [9] Xiao F, Wang ZG, Sun MB, Liang JH, Liu N. Large eddy simulation of liquid jet primary breakup in supersonic air crossflow. *Int J Multiphas Flow* 2016;87:229–40.
- [10] Herrmann M. A dual-scale LES subgrid model for turbulent liquid/gas phase interface dynamics. *13th Triennial international conference on liquid atomization and spray systems Tainan, Taiwan*; 2015.
- [11] Poinsot T, Veynante D. *Theoretical and numerical combustion*. 2nd ed. Irvine, CA, USA: Edwards; 2005.
- [12] Gorokhovski M, Herrmann M. Modeling primary atomization. *Annu Rev Fluid Mech* 2008;40:343–66.
- [13] Elghobashi S, Truesdell GC. On the two-way interaction between homogeneous turbulence and dispersed solid particles. I: turbulence modification. *Phys Fluids* 1993;5:1790.
- [14] Truesdell GC, Elghobashi S. On the two-way interaction between homogeneous turbulence and dispersed solid particles. II. Particle dispersion. *Phys Fluids* 1994;6:1405.
- [15] Pope SB. *Turbulent flows*. Cambridge University Press; 2011.
- [16] Escalapez L, Ma PC, Mayhew E, Xu R, Stouffer S, Lee T, Wang H, Ihme M. Fuel effects on lean blow-out in a realistic gas turbine combustor. *Combust Flame* 2017;181:82–99.
- [17] Som S, Aggarwal SK. Effects of primary breakup modeling on spray and combustion characteristics of compression ignition engines. *Combust Flame* 2010;157:1179–93.
- [18] Greenberg JB. Droplet size distribution effects in an edge flame with a fuel spray. *Combust Flame* 2017;179:228–37.
- [19] Sazhin SS. Advanced models of fuel droplet heating and evaporation. *Prog Energy Combust Sci* 2006;32:162–214.
- [20] Glimm J, Marchesin D, McBryan O. A numerical method for two phase flow with an unstable interface. *J Comput Phys* 1981;39:179–200.
- [21] Unverdi SO, Tryggvason G. A front-tracking method for viscous, incompressible, multi-fluid flows. *J Comput Phys* 1992;100:25–37.
- [22] Hirt CW, Nichols BD. Volume of fluid (VOF) method for the dynamics of free boundaries. *J Comput Phys* 1981;39:201–25.
- [23] Tryggvason G, Scardovelli R, Zaleski S. *Direct numerical simulations of gas-liquid multiphase flows*. Cambridge University press; 2011.
- [24] Osher S, Fedkiw R. *Level set methods and dynamic implicit surfaces*. Springer; 2002.
- [25] Sethian JA. Evolution, implementation, and application of level set and fast marching methods for advancing fronts. *J Comput Phys* 2011;169:503–55.
- [26] Osher S, Sethian JA. Fronts propagating with curvature dependent speed: algorithms based on Hamilton-Jacobi formulations. *J Comput Phys* 1988;79:12–49.
- [27] Gunstensen AK, Rothman DH, Zaleski S, Zanetti G. Lattice Boltzmann model of immiscible fluids. *Phys Rev A* 1991;43:4320–7.
- [28] Chen S, Doolen GD. Lattice Boltzmann method for fluid flows. *Annu Rev Fluid Mech* 1998;30:329–64.
- [29] Li Q, Luo KH, Kang QJ, He YL, Chen Q, Liu Q. Lattice Boltzmann methods for multiphase flow and phase-change heat transfer. *Prog Energy Combust Sci* 2016;52:62–105.
- [30] Wang ZB, Chen R, Wang H, Liao Q, Zhu X, Li SZ. An overview of smoothed particle hydrodynamics for simulating multiphase flow. *Appl Math Model* 2016;40(23–24):9625–55.
- [31] Marrone S, Colagrossi A, Le Touzé D, Graziani G. Fast free-surface detection and level-set function definition in SPH solvers. *J Comput Phys* 2010;229:3652–63.
- [32] Caginalp G, Fife P. Phase-field methods for interfacial boundaries. *Phys Rev B* 1986;33:7792–4.
- [33] Qin RS, Bhadeshia HK. Phase field method. *Mater Sci Tech* 2010;26:803–11.
- [34] Mirjalili S, Jain SS, Dodd MS. Interface-capturing methods for two-phase flows: an overview and recent developments. *Ann Res Briefs Center Turbul Res* 2017;117–35.
- [35] Albadawi A, Donoghue DB, Robinson AJ, Murray DB, Delaure YM. On the analysis of bubble growth and detachment at low Capillary and Bond numbers using Volume of Fluid and Level Set methods. *Chem Eng Sci* 2013;90:77–91.
- [36] Albadawi A, Donoghue DB, Robinson AJ, Murray DB, Delaure YM. Influence of surface tension implementation in Volume of Fluid and coupled Volume of Fluid with Level Set methods for bubble growth and detachment. *Int J Multiphase Flow* 2013;53:11–28.
- [37] Denner F, van der Heul DR, Oud GT, Villar MM, Neto A, Wachem BGM. Comparative study of mass-conserving interface capturing frameworks for two-phase flows with surface tension. *Int J Multiphase Flow* 2014;61:37–47.
- [38] Bilger C, Aboukhadr M, Vogiatzaki K, Cant RS. Evaluation of two-phase flow solvers using level set and volume of fluid methods. *J Comput Phys* 2017;345:665–86.
- [39] Losasso F, Fedkiw R, Osher S. Spatially adaptive techniques for level set methods and incompressible flow. *Comput Fluids* 2006;35:995–1010.
- [40] Gibou F, Fedkiw R, Osher S. A review of level-set methods and some recent applications. *J Comput Phys* 2018;353:82–109.
- [41] Osher S, Fedkiw RP. Level set methods: an overview and some recent results. *J Comput Phys* 2001;169:463–502.
- [42] Sethian JA, Smereka P. Level set methods for fluid interfaces. *Annu Rev Fluid Mech* 2003;35:341–72.
- [43] Sussman M, Smereka P, Osher S. A level set approach for computing solutions to incompressible two-phase flow. *J Comput Phys* 1994;114:146–59.
- [44] Sethian JA. *Level set methods and fast marching methods*. Cambridge University Press; 1999.
- [45] Nourgaliev RR, Wiri S, Dinh NT, Theofanous TG. On improving mass conservation of level set by reducing spatial discretization errors. *Int J Multiphas Flow* 2005;31:1329–36.
- [46] Salih A, Moulic SG. Some numerical studies of interface advection properties of level set method. *Sadhana* 2009;34:271–98.
- [47] Sheu TWH, Yu CH, Chiu PH. Development of a dispersively accurate conservative level set scheme for capturing interface in two-phase flows. *J Comput Phys* 2009;228:661–86.
- [48] Sheu TWH, Yu CH, Chiu PH. Development of level set method with good area preservation to predict interface in two-phase flows. *Int J Numer Meth Fluids* 2011;67:109–34.
- [49] Reed WH, Hill TR. *Triangular mesh methods for the neutron transport equation*, Los Alamos, NM: Los Alamos Scientific Laboratory; 1973. Tech Report LA-UR-73-479.
- [50] Rasitariner P, Hussaini MY. An efficient implicit discontinuous spectral Galerkin method. *J Comput Phys* 2001;172:718–38.
- [51] Remacle JF, Chevaugeon N, Marchandise A, Geuzaine C. Efficient visualization of high-order finite elements. *Int J Numer Methods Eng* 2007;69:750–71.
- [52] Owkes M, Desjardins O. A discontinuous Galerkin conservative level set scheme for interface capturing in multiphase flows. *J Comput Phys* 2013;249:275–302.
- [53] Chopp DL. Another look at velocity extensions in the level set method. *SIAM J Sci Comput* 2009;31:3255–73.
- [54] Enright D, Losasso F, Fedkiw R. A fast and accurate semi-Lagrangian particle level set method. *Comput Struct* 2005;83:479–90.
- [55] Strain J. Semi-Lagrangian methods for level set equations. *J Comput Phys* 1999;151:498–533.
- [56] Xiu D, Karniadakis GE. A semi-Lagrangian high-order method for Navier-Stokes equations. *J Comput Phys* 2001;172:658–84.
- [57] Desjardins O, Pitsch H. A spectrally refined interface approach for simulating multiphase flows. *J Comput Phys* 2009;228:1658–77.
- [58] Nave JC, Rosales RR, Seibold B. A gradient-augmented level set method with an optimally local, coherent advection scheme. *J Comput Phys* 2010;229:3802–27.

- [59] Lee C, Dolbow J, Mucha PJ. A narrow-band gradient-augmented level set method for multiphase incompressible flow. *J Comput Phys* 2014;273:12–37.
- [60] Kohn H, Nave JC. A new method for the level set equation using a hierarchical gradient truncation and remapping technique. *Comput Phys Commun* 2013;184:1547–54.
- [61] Adalsteinsson D, Sethian JA. The fast construction of extension velocities in level set methods. *J Comput Phys* 1999;148:2–22.
- [62] Ovsyannikov A, Sabelnikov V, Gorokhovski M. A new level set equation and its numerical assessments. In: Proceedings of the Summer Program. Center for Turbulence Research; 2012.
- [63] Sabelnikov V, Ovsyannikov AY, Gorokhovski M. Modified level set equation and its numerical assessment. *J Comput Phys* 2014;278:1–30.
- [64] Olsson E, Kreiss G. A conservative level set method for two phase flow. *J Comput Phys* 2005;210:225–46.
- [65] Olsson E, Kreiss G, Zahedi S. A conservative level set method for two phase flow II. *J Comput Phys* 2007;225:785–807.
- [66] Xiao F, Honma Y, Kono T. A simple algebraic interface capturing scheme using hyperbolic tangent function. *Int J Numer Meth Fluids* 2005;48:1023–40.
- [67] Walker C, Muller B. A conservative level set method for sharp interface multiphase flow simulation. *ECCOMAS CFD*; 2010.
- [68] Desjardins O, Moureau V, Pitsch H. An accurate conservative level set/ghost fluid method for simulating turbulent atomization. *J Comput Phys* 2008;227:8395–416.
- [69] Nonomura T, Kitamura K, Fujii K. A simple interface sharpening technique with a hyperbolic tangent function applied to compressible two-fluid modeling. *J Comput Phys* 2014;258:95–117.
- [70] Sussman M, Almgren AS, Bell JB, Colella P, Howell LH, Welcome ML. An adaptive level set approach for incompressible two-phase flows. *J Comput Phys* 1999;148:81–124.
- [71] Kim H, Liou MS. Accurate adaptive level set method and sharpening technique for three dimensional deforming interfaces. *Comput Fluids* 2011;44:111–29.
- [72] Herrmann M. A balanced force refined level set grid method for two-phase flows on unstructured flow solver grids. *J Comput Phys* 2008;227:2674–706.
- [73] Sussman M, Fatemi E, Smereka P, Osher S. An improved level set method for incompressible two-phase flows. *Comput Fluids* 1998;27:663–80.
- [74] Sussman M, Fatemi E. An efficient, interface-preserving level set redistancing algorithm and its application to interfacial incompressible fluid flow. *SIAM J Sci Comput* 1999;20:1165–91.
- [75] Russo G, Smereka P. A remark on computing distance functions. *J Comput Phys* 2000;163:51–67.
- [76] Hartmann D, Meinke M, Schröder W. Differential equation based constrained reinitialization for level set methods. *J Comput Phys* 2008;227:6821–45.
- [77] Hartmann D, Meinke M, Schröder W. The constrained reinitialization equation for level set methods. *J Comput Phys* 2010;229:1514–35.
- [78] Chang YC, Hou TY, Merriman B, Osher S. A level set formulation of Eulerian interface capturing methods for incompressible fluid flows. *J Comput Phys* 1996;124:449–64.
- [79] Merriman B, Bence JK, Osher SJ. Motion of multiple junctions: a level set approach. *J Comput Phys* 1994;112:334–63.
- [80] Chiu PH, Lin YT. A conservative phase field method for solving incompressible two-phase flows. *J Comput Phys* 2011;230:185–204.
- [81] McCaslin LO, Desjardins O. A localized re-initialization equation for the conservative level set method. *J Comput Phys* 2014;262:408–26.
- [82] Ausas RF, Dari EA, Buscaglia GC. A geometric mass-preserving redistancing scheme for the level set function. *Int J Numer Meth Fluids* 2011;65:989–1010.
- [83] Salih A, Moulic G. A mass conservation scheme for level set method applied to multiphase incompressible flows. *Int J Comput Meth Eng Sci Mech* 2013;14:271–89.
- [84] Sussman M, Puckett EG. A coupled level set and volume-of-fluid method for computing 3D and axisymmetric incompressible two-phase flows. *J Comput Phys* 2000;162:301–37.
- [85] Sussman M. A second order coupled level set and volume-of-fluid method for computing growth and collapse of vapor bubbles. *J Comput Phys* 2003;187:110–36.
- [86] Son G. Efficient implementation of a coupled level-set and volume-of-fluid method for three dimensional incompressible two-phase flows. *Numer Heat Tr-B Fund* 2003;43:549–65.
- [87] Yang X, James AJ, Lowengrub J, Zheng X, Cristini V. An adaptive coupled level-set/volume-of-fluid interface capturing method for unstructured triangular grids. *J Comput Phys* 2006;217:364–94.
- [88] Menard T, Tanguy S, Berlemont A. Coupling level set/VOF/ghost fluid methods: validation and application to 3D simulation of the primary break-up of a liquid jet. *Int J Multiphas Flow* 2007;33:510–24.
- [89] Lv X, Zou Q, Zhao Y, Reeve D. A novel coupled level set and volume of fluid method for sharp interface capturing on 3D tetrahedral grids. *J Comput Phys* 2010;229:2573–604.
- [90] Wang Z, Yang J, Stern F. A new volume-of-fluid method with a constructed distance function on general structured grids. *J Comput Phys* 2012;231:3703–22.
- [91] Wang Z, Tong AY. A sharp surface tension modeling method for two-phase incompressible interfacial flows. *Int J Numer Meth Fluids* 2010;64:709–32.
- [92] Sun DL, Tao WQ. A coupled volume-of-fluid and level set (VOSET) method for computing incompressible two-phase flows. *Int J Heat Mass Tran* 2010;53:645–55.
- [93] Kees CE, Akkerman I, Farthing MW, Bazilevs Y. A conservative level set method suitable for variable-order approximations and unstructured meshes. *J Comput Phys* 2011;230:4536–58.
- [94] Wang Y, Simakhina S, Sussman M. A hybrid level set-volume constraint method for incompressible two-phase flow. *J Comput Phys* 2012;231:6438–71.
- [95] van der Pijl SP, Segal A, Vuik C, Wesseling P. A mass-conserving level-set method for modeling of multi-phase flows. *Int J Numer Meth Fluids* 2005;47:339–61.
- [96] van der Pijl SP, Segal A, Vuik C, Wesseling P. Computing three-dimensional two-phase flows with a mass-conserving level set method. *Comput Visual Sci* 2008;11:221–35.
- [97] Luo K, Shao CX, Yang Y, Fan JR. A mass conserving level set method for detailed numerical simulation of liquid atomization. *J Comput Phys* 2015;298:495–519.
- [98] Chai M, Luo K, Shao CX, Fan JR. An efficient level set remedy approach for simulations of two-phase flow based on sigmoid function. *Chem Eng Sci* 2017;172:335–52.
- [99] Enright D, Fedkiw R, Ferziger J, Mitchell I. A hybrid particle level set method for improved interface capturing. *J Comput Phys* 2002;183:83–116.
- [100] Hieber SE, Koumoutsakos P. A Lagrangian particle level set method. *J Comput Phys* 2005;210:342–67.
- [101] Trontin P, Vincent S, Estivalezes JL, Caltagirone JP. A subgrid computation of the curvature by a particle/level set method. Application to a front-tracking/ ghost-fluid method for incompressible flows. *J Comput Phys* 2012;231:6990–7010.
- [102] Wang ZY, Yang JM, Stern F. Comparison of particle level set and CLSVOF methods for interfacial flows. 46th AIAA aerospace sciences meeting and exhibit, 7–10 January, Reno, Nevada; 2008.
- [103] Gomes J, Faugeras O. Reconciling distance functions and Level Sets. *J Vis Commun Image R* 2000;11:209–23.
- [104] Li C, Xu C, Gui C, Fox MD. Level set evolution without re-initialization: a new variational formulation. In: CVPR, 1; 2005. p. 430–6.
- [105] Zhao H, Chan T, Merriman B, Osher S. A variational level set approach to multiphase motion. *J Comput Phys* 1996;127:179–95.
- [106] Boudaoust M, Otmani R, Benhadid H. Conservative level set method without re-initialization process: application to multiphase flows. *Int J Simul Model* 2013;33:162–72.
- [107] Touré MK, Soulaïmani A. Stabilized finite element methods for solving the level set equation without reinitialization. *Comput Math Appl* 2016;71:1602–23.
- [108] Li C, Xu C, Gui C, Fox MD. Distance regularized level set evolution and its application to image segmentation. *IEEE Trans Image Process* 2010;19:3243–54.
- [109] Cummins SJ, Francois MM, Kothe DB. Estimating curvature from volume fractions. *Comput Struct* 2005;83:425–34.
- [110] Pai MG, Pitsch H, Desjardins O. Detailed numerical simulations of primary atomization of liquid jets in crossflow. 47th AIAA Aerospace sciences meeting including the new horizons forum and aerospace exposition; 2009.
- [111] Shao CX, Luo K, Yang Y, Fan JR. Detailed numerical simulation of swirling primary atomization using a mass conserving level set method. *Int J Multiphas Flow* 2017;89:57–68.
- [112] Popinet S. Numerical models of surface tension. *Annu Rev Fluid Mech* 2018;50:49–75.
- [113] Desjardins O, Moureau V. Methods for multiphase flows with high density ratio. Center for Turbulence Research; 2010.
- [114] Scardovelli R, Zaleski S. Direct numerical simulation of free-surface and interfacial flow. *Annu Rev Fluid Mech* 1999;31:567–603.
- [115] Lalanne B, Villegas LR, Tanguy S, Risso F. On the computation of viscous terms for incompressible two-phase flows with Level Set/Ghost Fluid Method. *J Comput Phys* 2015;301:289–307.
- [116] LeVeque RJ, Li Z. Immersed interface methods for Stokes flow with elastic boundaries or surface tension. *SIAM J Sci Comput* 1997;18:709–35.
- [117] Tanguy SB, Sagan ML, Lalanne B, Couderc FDR, Colin C. Benchmarks and numerical methods for the simulation of boiling flows. *J Comput Phys* 2014;264:1–22.
- [118] Kang M, Fedkiw RP, Liu XD. A boundary condition capturing method for multiphase incompressible flow. *J Sci Comput* 2000;15:323–60.
- [119] Tanguy S, Menard T, Berlemont A. A level set method for vaporizing two-phase flows. *J Comp Phys* 2007;221:837–53.
- [120] Papac J, Gibou F, Ratsch C. Efficient symmetric discretization for the Poisson, heat and Stefan problems with Robin boundary conditions. *J Comput Phys* 2010;229:875–89.
- [121] Fedkiw RP, Aslam T, Merriman B, Osher S. A non-oscillatory Eulerian approach to interfaces in multimaterial flows (the ghost fluid method). *J Comput Phys* 1999;152:457–92.
- [122] Nguyen DQ, Fedkiw RP, Kang M. A boundary condition capturing method for incompressible flame discontinuities. *J Comput Phys* 2001;172:71–98.
- [123] Gjennestad MA. Modeling of heat transfer in two-phase flow using the level-set method. Trondheim: Norwegian University of Science and Technology; 2013.
- [124] Gibou F, Fedkiw RP, Cheng L, Kang M. A second-order-accurate symmetric discretization of the Poisson equation on irregular domains. *J Comput Phys* 2002;176:205–27.
- [125] Wang X, Jackson TL, Massa L. Numerical simulation of heterogeneous propellant combustion by a level set method. *Combust Theor Model* 2004;8:227–54.
- [126] Shaikh J, Sharma A, Bhardwaj R. On sharp-interface level-set method for heat and/or mass transfer induced Stefan problem. *Int J Heat Mass Tran* 2016;96:458–73.

- [127] Houim RW, Kuo KK. A ghost fluid method for compressible reacting flows with phase change. *J Comput Phys* 2013;235:865–900.
- [128] Liu XD, Fedkiw RP, Kang MJ. A boundary condition capturing method for Poisson's equation on irregular domains. *J Comput Phys* 2000;160:151–78.
- [129] Gibou F, Fedkiw R. A fourth order accurate discretization for the Laplace and heat equations on arbitrary domains, with applications to the Stefan problem. *J Comput Phys* 2005;202:577–601.
- [130] Ng YT, Min C, Gibou F. An efficient fluid-solid coupling algorithm for single-phase flows. *J Comput Phys* 2009;228:8807–29.
- [131] Papac J, Helgadottir A, Ratsch C, Gibou F. A level set approach for diffusion and Stefan-type problems with Robin boundary conditions on quadtree/octree adaptive Cartesian grids. *J Comput Phys* 2013;233:241–61.
- [132] Helgadóttir Á, Ng YT, Min C, Gibou F. Imposing mixed Dirichlet-Neumann-Robin boundary conditions in a level-set framework. *Comput Fluids* 2015;121:68–80.
- [133] Gibou F, Chen L, Nguyen D, Banerjee S. A level set based sharp interface method for the multiphase incompressible Navier-Stokes equations with phase change. *J Comp Phys* 2007;222:536–55.
- [134] Aslam TD. A partial differential equation approach to multidimensional extrapolation. *J Comput Phys* 2004;193:349–55.
- [135] McCaslin JO, Courtnie E, Desjardins O. A fast marching approach to multidimensional extrapolation. *J Comput Phys* 2014;274:393–412.
- [136] Chorin AJ. A numerical method for solving incompressible viscous flow problems. *J Comput Phys* 1967;2(1):12–26.
- [137] Villegas LR, Tanguy S, Castanet G, Caballina O, Lemoine F. Direct numerical simulation of the impact of a droplet onto a hot surface above the Leidenfrost temperature. *Int J Heat Mass Tran* 2017;104:1090–109.
- [138] Lee MS, Riaz A, Aute V. Direct numerical simulation of incompressible multi-phase flow with phase change. *J Comput Phys* 2017;344:381–418.
- [139] Strotos G, Gavaises M, Theodorakatos A, Bergeles G. Numerical investigation of the evaporation of two-component droplets. *Fuel* 2011;90:1492–507.
- [140] Miller RS, Harstad K, Bellan J. Evaluation of equilibrium and non-equilibrium evaporation models for many-droplet gas-liquid flow simulations. *Int J Multiphas Flow* 1998;24:1025–55.
- [141] Chai M, Luo K, Shao CX, Wang HO, Fan JR. A coupled vaporization model based on temperature/species gradients for detailed numerical simulations using conservative level set method. *Int J Heat Mass Tran* 2018;127:743–60.
- [142] Shao CX, Luo K, Chai M, Wang HO, Fan JR. A computational framework for interface-resolved DNS of simultaneous atomization, evaporation and combustion. *J Comp Phys* 2018;371:751–78.
- [143] Son G. A level-set method for analysis of microdroplet evaporation on a heated surface. *J Mech Sci Technol* 2010;24:991–7.
- [144] Villegas LR, Alis R, Lepilliez M, Tanguy S. A Ghost Fluid/Level Set Method for boiling flows and liquid evaporation: application to the Leidenfrost effect. *J Comput Phys* 2016;316:789–813.
- [145] Irfan M, Muradoglu M. A front tracking method for particle-resolved simulation of evaporation and combustion of a fuel droplet. *Comput Fluids* 2018;174:283–99.
- [146] Kim D, Desjardins O, Herrmann M, Moin P. Toward two-phase simulation of the primary breakup of a round liquid jet by a coaxial flow of gas. Center for Turbulence Research; 2006. Annual Research Briefs.
- [147] Kim D, Moin P. Numerical simulation of the breakup of a round liquid jet by a coaxial flow of gas with a subgrid Lagrangian breakup model. Center for Turbulence Research; 2011. Annual Research Briefs.
- [148] Marmottant P, Villermaux E. On spray formation. *J Fluid Mech* 2004;498:73–111.
- [149] Herrmann M, Gorokhovski M. An outline of an LES subgrid model for liquid/gas phase interface dynamics. In: Proceedings of the summer program. Center for Turbulence Research; 2008.
- [150] Herrmann M. A parallel Eulerian interface tracking/Lagrangian point particle multi-scale coupling procedure. *J Comput Phys* 2010;229:745–59.
- [151] Herrmann M. On simulating primary atomization using the refined level set grid method. *ILASS Americas 21st annual conference on liquid atomization and spray systems*; 2008.
- [152] Shinjo J, Umemura A. Simulation of liquid jet primary breakup: dynamics of ligament and droplet formation. *Int J Multiphas Flow* 2010;36:513–32.
- [153] Shinjo J, Umemura A. Detailed simulation of primary atomization mechanisms in Diesel jet sprays (isolated identification of liquid jet tip effects). *Proc Combust Inst* 2011;33:2089–97.
- [154] Shinjo J, Umemura A. Surface instability and primary atomization characteristics of straight liquid jet sprays. *Int J Multiphas Flow* 2011;37:1294–304.
- [155] Desjardins O, McCaslin JO, Owkes M, Brady P. Direct numerical and large-eddy simulation of primary atomization in complex geometries. *Atomization Spray* 2013;23:1001–48.
- [156] Desjardins O, Pitsch H. Detailed numerical investigation of turbulent atomization of liquid jets. *Atomization Spray* 2010;20:311–36.
- [157] McCaslin JO, Desjardins O. Numerical investigation of primary air-blast atomization and modal analysis of flow instabilities. *AIAA SciTech, 52nd aerospace sciences meeting*; 2014.
- [158] Lebas R, Ménard T, Beau PA, Berlemont A, Demoulin FX. Numerical simulation of primary break-up and atomization: DNS and modeling study. *Int J Multiphas Flow* 2009;35:247–60.
- [159] Demoulin FX, Reveillon J, Duret B, Bouali Z, Desjonquieres P, Ménard T. Toward using direct numerical simulation to improve primary break-up modeling. *Atomization Spray* 2013;23:957–80.
- [160] Cousin J, Berlemont A, Ménard T, Grout S. Primary breakup simulation of a liquid jet discharged by a low-pressure compound nozzle. *Comput Fluids* 2012;63:165–73.
- [161] Arienti M, Sussman M. An embedded level set method for sharp-interface multiphase simulations of diesel injectors. *Int J Multiphas Flow* 2014;59:1–14.
- [162] Chenadec VL, Pitsch H. A conservative framework for primary atomization computation and application to the study of nozzle and density ratio effects. *Atomization Spray* 2013;23:1139–65.
- [163] Tomar G, Fuster D, Zaleski S, Popinet S. Multiscale simulations of primary atomization. *Comput Fluids* 2010;39:1864–74.
- [164] Jarrahbashi D, Sirignano WA. Vorticity dynamics for transient high-pressure liquid injection. *Phys Fluids* 2014;26:101304.
- [165] Jarrahbashi D, Sirignano WA, Popov PP, Hussain F. Early spray development at high gas density: hole, ligament and bridge formations. *J Fluid Mech* 2016;792:186–231.
- [166] Zandian A, Sirignano WA, Hussain F. Planar liquid jet: early deformation and atomization cascades. *Phys Fluids* 2017;29:062109.
- [167] Zandian A, Sirignano WA, Hussain F. Understanding liquid-jet atomization cascades via vortex dynamics. *J Fluid Mech* 2018;843:293–354.
- [168] Herrmann M. Detailed numerical simulations of the primary atomization of a turbulent liquid jet in crossflow. *J Eng Gas Turb Power* 2010;132:061506–1–10.
- [169] Herrmann M. Detailed simulations of the breakup processes of turbulent liquid jets in subsonic crossflows. *11th Triennial international annual conference on liquid atomization and spray systems, ICCLASS*; 2009.
- [170] Brown CT, McDonell VG. Near field behavior of a liquid jet in a crossflow. *Proc Annua Conf ILASS Americas*. ILASS Americas; 2006.
- [171] Herrmann M, Arienti M, Soteriou M. The impact of density ratio on the liquid core dynamics of a turbulent liquid jet injected into a crossflow. *J Eng Gas Turb Power* 2011;133:061501–1–9.
- [172] Herrmann M. The influence of density ratio on the primary atomization of a turbulent liquid jet in crossflow. *Proc Combust Inst* 2011;33:2079–88.
- [173] Behzad M, Ashgriz N, Karney BW. Surface breakup of a non-turbulent liquid jet injected into a high pressure gaseous crossflow. *Int J Multiphas Flow* 2016;80:100–17.
- [174] Behzad M, Ashgriz N, Mashayek A. Azimuthal shear instability of a liquid jet injected into a gaseous cross-flow. *J Fluid Mech* 2015;767:146–72.
- [175] Owkes M, Desjardins O. Large-eddy simulation study of injector geometry on liquid jet in cross-flow and validation with experiments. *AIAA SciTech, 52nd aerospace sciences meeting*; 2014.
- [176] Pai MG, Moreno IB, Desjardins O, Pitsch H. Role of Weber number in primary breakup of turbulent liquid jets in crossflow. Center for Turbulence Research; 2009. Annual Research Briefs.
- [177] Li X, Soteriou MC. High fidelity simulation and analysis of liquid jet atomization in a gaseous crossflow at intermediate Weber number. *Phys Fluids* 2016;28:082101.
- [178] Li X, Soteriou MC, Arienti M, Sussman MM. High-fidelity simulation of atomization and evaporation in a liquid jet in cross-flow. *49th AIAA aerospace sciences meeting including the new horizons forum and aerospace exposition*; 2011.
- [179] Arienti M, Li X, Soteriou MC, Eckett CA, Sussman M, Jensen RJ. Coupled level-set/volume-of-fluid method for simulation of injector atomization. *J Propul Power* 2013;29:147–57.
- [180] Chen X, Ma D, Yang V, Popinet S. High-fidelity simulations of impinging jet atomization. *Atomization Spray* 2013;23:1079–101.
- [181] Ma D, Chen X, Khare P, Yang V. Atomization patterns and breakup characteristics of liquid sheets formed by two impinging jets. *49th AIAA aerospace sciences meeting including the new horizons forum and aerospace exposition*; 2011.
- [182] Li X, Soteriou MC. High-fidelity simulation of fuel atomization in a realistic swirling flow injector. *Atomization Spray* 2013;23:1049–78.
- [183] Li X, Soteriou MC, Kim W, Cohen JM. High fidelity simulation of the spray generated by a realistic swirling flow injector. *J Eng Gas Turb Power* 2014;136:071503–1–10.
- [184] Fuster D, Bagué A, Boeck T, Moyne LL, Leboissetter A, Popinet S, Ray P, Scardovelli R, Zaleski S. Simulation of primary atomization with an octree adaptive mesh refinement and VOF method. *Int J Multiphas Flow* 2009;35:550–65.
- [185] Shao CX, Luo K, Chai M, Fan JR. Sheet, ligament and droplet formation in swirling primary atomization. *AIP Adv* 2018;8:045211.
- [186] Epstein B. Logarithmic-normal distribution in breakage of solids. *Ind Eng Chem Res* 1948;40:2289–91.
- [187] Guildenbecher DR, Lopez-Rivera C, Sojka PE. Secondary atomization. *Exp Fluids* 2009;46:371–402.
- [188] Balabel A, Binninger B, Herrmann M, Peters N. Calculation of droplet deformation by surface tension effects using the level set method. *Combust Sci Technol* 2002;174:257–78.
- [189] Ni MJ, Komori S, Morley NB. Direct simulation of falling droplet in a closed channel. *Int J Heat Mass Trans* 2006;49:366–76.
- [190] Liu J, Xu X. Direct numerical simulation of secondary breakup of liquid drops. *Chin J Aeronaut* 2010;23:153–61.
- [191] Xiao F, Dianat M, McGuirk JJ. A robust interface method for drop formation and breakup simulation at high density ratio using an extrapolated liquid velocity. *Comput Fluids* 2016;136:402–20.
- [192] Xiao F, Wang ZG, Sun MB, Liu N, Yang X. Simulation of drop deformation and breakup in supersonic flow. *Proc Combust Inst* 2018;36:2417–24.
- [193] Yang W, Jia M, Che ZZ, Sun K, Wang TY. Transitions of deformation to bag breakup and bag to bag-stamen breakup for droplets subjected to a continuous gas flow. *Int J Heat Mass Trans* 2017;111:884–94.

- [194] Yang W, Jia M, Sun K, Wang TY. Influence of density ratio on the secondary atomization of liquid droplets under highly unstable conditions. *Fuel* 2016;174:25–35.
- [195] Aalburg C, Van Leer B, Faeth GM. Deformation and drag properties of round drops subjected to shock-wave disturbances. *AIAA J* 2003;41:2371–8.
- [196] Suh Y, Lee C. A numerical method for the calculation of drag and lift of a deformable droplet in shear flow. *J Comp Phys* 2013;241:35–57.
- [197] Shao CX, Luo K, Fan JR. Detailed numerical simulation of unsteady drag coefficient of deformable droplet. *Chem Eng J* 2017;308:619–31.
- [198] Qian J, Law CK. Regimes of coalescence and separation in droplet collision. *J Fluid Mech* 1997;331:59–80.
- [199] Tanguy S, Berlenont A. Application of a level set method for simulation of droplet collisions. *Int J Multiphas Flow* 2005;31:1015–35.
- [200] Ashgriz N, Poo JV. Coalescence and separation in binary collisions of liquid drops. *J Fluid Mech* 1990;221:183–204.
- [201] Pan Y, Suga K. Numerical simulation of binary liquid droplet collision. *Phys Fluids* 2005;17:082105.
- [202] Balabel A. Numerical simulation of two-dimensional binary droplets collision outcomes using the level set method. *Int J Comput Fluid D* 2012;26:1–21.
- [203] Kwakkel M, Breugem WP, Boersma BJ. Extension of a CLSVOF method for droplet-laden flows with a coalescence/breakup model. *J Comp Phys* 2013;253:166–88.
- [204] Balcazar N, Lehmkuhl O, Rigola J, Oliva A. A multiple marker level-set method for simulation of deformable fluid particles. *Int J Multiphas Flow* 2015;74:125–42.
- [205] Yarin AL. Drop impact dynamics: splashing, spreading, receding, bouncing... *Annu Rev Fluid Mech* 2006;38:159–92.
- [206] Yokoi K. A numerical method for free-surface flows and its application to droplet impact on a thin liquid layer. *J Sci Comput* 2008;35:372–96.
- [207] Coyajee E, Boersma BJ. Numerical simulation of drop impact on a liquid-liquid interface with a multiple marker front-capturing method. *J Comp Phys* 2009;228:4444–67.
- [208] Rieber M, Frohn A. A numerical study on the mechanism of splashing. *Int J Heat Fluid Flow* 1999;20:455–61.
- [209] Shin S, Chergui J, Juric D. A solver for massively parallel direct numerical simulation of three-dimensional multiphase flows. *J Mech Sci Technol* 2017;31:1739–51.
- [210] Lee SH, Hur N, Kang S. A numerical analysis of drop impact on liquid film by using a level set method. *J Mech Sci Technol* 2011;25:2567–72.
- [211] Liang GT, Guo YL, Shen SQ, Yang Y. Crown behavior and bubble entrainment during a drop impact on a liquid film. *Theor Comput Fluid Dyn* 2014;28:159–70.
- [212] Guo YL, Wei L, Liang GT, Shen SQ. Simulation of droplet impact on liquid film with CLSVOF. *Int J Heat Mass Tran* 2014;53:26–33.
- [213] Chai M, Luo K, Shao CX, Chen S, Fan JR. DNS analysis of incipient drop impact dynamics using an accurate level set method. *Chin J Chem Eng* 2017;25:1–10.
- [214] Liu XH, Zhao YM, Chen S, Shen SQ, Zhao XY. Numerical research on the dynamic characteristics of a droplet impacting a hydrophobic tube. *Phys Fluids* 2017;29:062105.
- [215] Yan Z, Li Y. A comprehensive study of dynamic and heat transfer characteristics of droplet impact on micro-scale rectangular grooved surface. *Energies* 2018;11:1390.
- [216] Liang GT, Mudawar I. Review of mass and momentum interactions during drop impact on a liquid film. *Int J Heat Mass Tran* 2016;101:577–99.
- [217] Elghobashi S. DNS of turbulent flows laden with droplets or bubbles. *Annu Rev Fluid Mech* 2019;51:217–44.
- [218] Li Z, Jaberi FA. Turbulence-interface interactions in a two-fluid homogeneous flow. *Phys Fluids* 2009;21:095102.
- [219] Trontin P, Vincent S, Estivalezes JL, Caltagirone JP. Direct numerical simulation of a freely decaying turbulent interfacial flow. *Intl J Multiphas Flow* 2010;36:891–907.
- [220] Shao CX, Luo K, Yang Y, Fan JR. Direct numerical simulation of droplet breakup in homogeneous isotropic turbulence: the effect of the Weber number. *Int J Multiphas Flow* 2018;107:263–74.
- [221] Duret B, Luret G, Reveillon J, Menard T, Berlemont A, Demoulin FX. DNS analysis of turbulent mixing in two-phase flows. *Int J Multiphas Flow* 2012;40:93–105.
- [222] Duret B, Reveillon J, Menard T, Demoulin FX. Improving primary atomization modeling through DNS of two-phase flows. *Intl J Multiphas Flow* 2013;55:130–7.
- [223] Ling Y, Zaleski S. Multi-scale simulation of atomization with small drops represented by Lagrangian Point-Particle Model. *Int J Multiphas Flow* 2015;76:122–43.
- [224] Zuzio D, Estivalezes JL, DiPierro B. An improved multiscale Eulerian-Lagrangian method for simulation of atomization process. *Comput Fluids* 2017;100:1–17.
- [225] Gottfried BS, Lee CJ, Bell KJ. The Leidenfrost phenomenon: film boiling of liquid droplets on a flat plate. *Int J Heat Mass Tran* 1966;9:1167–87.
- [226] Ge Y, Fan LS. Three-dimensional simulation of impingement of a liquid droplet on a flat surface in the Leidenfrost regime. *Phys Fluids* 2005;17:027104.
- [227] Ge Y, Fan LS. 3-D modeling of the dynamics and heat transfer characteristics of subcooled droplet impact on a surface with film boiling. *Int J Heat Mass Tran* 2006;49:4231–49.
- [228] Ge Y, Fan LS. Three-dimensional direct numerical simulation for film-boiling contact of moving particle and liquid droplet. *Phys Fluids* 2006;18:117104.
- [229] Ge Y, Fan LS. Droplet-particle collision mechanism with film-boiling evaporation. *J Fluid Mech* 2007;573:311–37.
- [230] Chatzikyriakou D, Walker SP, Hewitt GF, Narayanan C, Lakehal D. Comparison of measured and modelled droplet-hot wall interactions. *Appl Therm Eng* 2009;29:1398–405.
- [231] Son G. A sharp-interface level-set method for analysis of Marangoni effect on microdroplet evaporation. *Int Commun Heat Mass* 2014;58:156–65.
- [232] Lee J, Son G. A level-set method for analysis of particle motion in an evaporating microdroplet. *Numer Heat Transfer B-Fund* 2015;67:25–46.
- [233] Son G. Numerical simulation of particle-laden droplet evaporation with the Marangoni effect. *Eur Phys J Special Top* 2015;224:401–13.
- [234] Fechter S, Munz CD, Rohde C, Zeiler C. Approximate Riemann solver for compressible liquid vapor flow with phase transition and surface tension. *Comput Fluids* 2018;169:169–85.
- [235] Zoby MRG, Navarro-Martinez S, Kronenburg A, Marquis AJ. Evaporation rates of droplet arrays in turbulent reacting flows. *Proc Combust Inst* 2011;33:2117–25.
- [236] Haruki Y, Pillai AL, Kitano T, Kurose P. Numerical investigation of flame propagation in fuel droplet arrays. *Atomization Spray* 2018;28:357–88.
- [237] Shinjo J, Umemura A. Droplet/turbulence interaction and early flame kernel development in an autoigniting realistic dense spray. *Proc Combust Inst* 2013;34:1553–60.
- [238] Shinjo J, Xia J, Umemura A. Droplet/ligament modulation of local small-scale turbulence and scalar mixing in a dense fuel spray. *Proc Combust Inst* 2015;35:1595–602.
- [239] Shinjo J, Xia J, Ganippa LC, Megaritis A. Physics of puffing and microexplosion of emulsion fuel droplets. *Phys Fluids* 2014;26:103302.
- [240] Shinjo J, Xia J, Megaritis A, Ganippa LC, Cracknell RF. Modeling temperature distribution inside an emulsion fuel droplet under convective heating: a key to predicting microexplosion and puffing. *Atomization Spray* 2016;26:551–83.
- [241] Huang A, Joseph DD. Stability of liquid-vapor flow down an inclined channel with phase change. *Int J Heat Mass Tran* 1993;36:663–72.
- [242] Shankar PN, Deshpande MD. On the temperature distribution in liquid-vapor phase change between plane liquid surfaces. *Phys Fluids A* 1990;2:1030–8.
- [243] Huang A, Joseph DD. Instability of the equilibrium of a liquid below its vapour between horizontal heated plates. *J Fluid Mech* 1992;242:235–47.
- [244] Juric D, Tryggvason G. Computations of boiling flows. *Int J Multiphas Flow* 1998;24:387–410.



Kun Luo is a full professor in the State Key Laboratory of Clean Energy Utilization at Zhejiang University, China since 2010. He received his B.S.E. from Wuhan University in 2000, and his Ph.D. from Zhejiang University in 2005. From 2007 to 2009, he worked at the Center for Turbulence Research, Stanford University as a postdoctoral fellow. Prof. Luo's research centers on Computational Energy Sciences with high-fidelity simulations on complex multiphase flows and combustion in energy and power system. He and his students have developed a number of algorithms, codes, and multi-physics simulation platforms for studying reacting/non-reacting two-phase flows towards efficient and clean energy utilization. In these endeavors, Prof. Luo has undertaken over 10 projects as the principal investigator, and authored or co-authored more than 150 technical papers in international peer-review journals. Prof. Luo has won the Distinguished Paper Award from the 33rd International Symposium on Combustion and the Wu Zhonghua Excellent Young Scholar Award from Chinese Association of Engineering Thermal Physics in 2011. He is an Associate Editor of the *Canadian Journal of Chemical Engineering*, an Editorial Board member of *International Journal of Spray and Combustion Dynamics*, and an Editorial Advisory Board member of *International Journal of Multiphase Flow*.



Changxiao Shao is currently working as a postdoctoral fellow in the State Key Laboratory of Clean Energy Utilization at Zhejiang University, China. He received his B.E. degree in School of Power and Mechanical Engineering at Wuhan University in 2012 and Ph.D degree in College of Energy Engineering at Zhejiang University in 2017. His doctoral research focused on the detailed numerical simulation of swirling primary atomization. He and his colleagues have developed a new mass conserving level set method for capturing the gas-liquid interface and explored corresponding mechanism of swirling primary atomization. He has also participated in five projects as the major investigator, and authored or co-authored over 10 technical papers in international journals. He won the Distinguished Paper Award of Chen Xuejun young scholars in multiphase annual meeting by the Chinese Society of Engineering Thermophysics in 2016. His current research includes developing computational framework for interface-resolved simulations of simultaneous atomization/evaporation/combustion and investigating the interactions among evaporating droplets and turbulence in turbulent flows.



Min Chai received his B.E. degree from Nanjing University of Science and Technology, China in 2014. Since then, he has been a Ph.D candidate in the State Key Laboratory of Clean Energy Utilization at Zhejiang University. His doctoral research focused on interface-resolved detailed numerical simulations of gas-liquid flows (including liquid breakup, phase change and combustion). He and his colleagues have developed several numerical methods and a simulation platform for studying reacting and non-reacting gas-liquid flows. He has also participated in three projects as a major investigator, and authored or co-authored 6 technical papers in international journals.



Jianren Fan is a Cheung Kong Scholar Professor in the Department of Energy, Zhejiang University. He received his B. S. degree from Xi'an Jiaotong University of China in 1981 and PhD degree from the Department of Mechanical Engineering, Technical University of Vienna, Austria in 1984. His current research includes numerical simulation and experimental studies on gas-solid two-phase flows and combustion. Direct numerical simulation (DNS), large eddy simulation (LES) and PIV techniques are developed to investigate turbulent coherent structures, particle dispersion, spray atomization, turbulence modulation, particle-particle interactions, heat/mass transfer and chemical reaction in turbulent flows. Theoretical and experimental investigations of nano-fluid and fuel cell have also been performed. He is a Member of Board of Directors of the Chinese Society of Thermophysics, a Member of Editorial Board of Frontiers of Energy and Power Engineering in China, Journal of Hydrodynamics, Journal of Engineering Thermophysics, and Journal of Zhejiang University (Science). He was awarded the Second-classs Prize of the National Natural Science of China in 2005.